NANO · MICRO small
www.small-journal.com

Smart Adsorbents for Aquatic Environmental Remediation

Ehsan Nazarzadeh Zare, Ackmez Mudhoo, Moonis Ali Khan, Marta Otero, Zumar Muhammad Ali Bundhoo, Manvendra Patel, Anju Srivastava, Chanaka Navarathna, Todd Mlsna, Dinesh Mohan, Charles U. Pittman Jr., Pooyan Makvandi, and Mika Sillanpää**

A noticeable interest and steady rise in research studies reporting the design and assessment of smart adsorbents for sequestering aqueous metal ions and xenobiotics has occurred in the last decade. This motivates compiling and reviewing the characteristics, potentials, and performances of this new adsorbent generation's metal ion and xenobiotics sequestration. Herein, stimuli-responsive adsorbents that respond to its media (as internal triggers; e.g., pH and temperature) or external triggers (e.g., magnetic field and light) are highlighted. Readers are then introduced to selective adsorbents that selectively capture materials of interest. This is followed by a discussion of self-healing and self-cleaning adsorbents. Finally, the review ends with research gaps in material designs.

1. Introduction

The penetration and persistence of anthropogenic metals ions[1,2] and organic xenobiotics[3–12] into the natural waters continue to remain severe environmental health and ecosystem-related issues. Cytotoxic pollutants have long-lasting noxious metabolic effects on living organisms,[13,14] eventually leading to toxicity,[15,16] and mortality.[17,18] There are several techniques that have been employed for removal of pollutants from wastewater including, amongst others, traditional filtration, coagulation/flocculation, membrane-utilizing

E. Nazarzadeh Zare
School of Chemistry
Damghan University
Damghan 36716-41167, Iran

A. Mudhoo
Department of Chemical and Environmental Engineering
Faculty of Engineering
University of Mauritius
Réduit, Moka 80837, Mauritius

M. Ali Khan, M. Sillanpää
Chemistry Department
College of Science
King Saud University
Riyadh 11451, Saudi Arabia
E-mail: mikaetapiosillanpaa@duytan.edu.vn

M. Otero
CESAM—Centre for Environmental and Marine Studies
Department of Environment and Planning
University of Aveiro
Campus de Santiago, Aveiro 3810-193, Portugal

Z. M. A. Bundhoo
Energy and Environment Consultant
Phoenix 73622, Mauritius

M. Patel, D. Mohan
School of Environmental Sciences
Jawaharlal Nehru University
New Delhi 110067, India

A. Srivastava
Chemistry Department
Hindu College
University of Delhi
Delhi 110007, India

C. Navarathna, T. Mlsna, C. U. Pittman Jr.
Department of Chemistry
Mississippi State University
Mississippi State, MS 39762, USA

P. Makvandi
Istituto Italiano di Tecnologia
Centre for Materials Interface
Viale Rinaldo Piaggio 34, Pontedera, Pisa 56025, Italy
E-mail: pooyanmakvandi@gmail.com, Pooyan.makvandi@iit.it

M. Sillanpää
Department of Chemical Engineering
School of Mining
Metallurgy and Chemical Engineering
University of Johannesburg
P. O. Box 17011, Doornfontein 2028, South Africa

M. Sillanpää
School of Chemical and Metallurgical Engineering
University of the Witwatersrand
Johannesburg 2050, South Africa

M. Sillanpää
School of Resources and Environment
University of Electronic Science and Technology of China (UESTC)
NO. 2006, Xiyuan Ave., West High-Tech Zone, Chengdu, Sichuan 611731, P.R. China

M. Sillanpää
Faculty of Science and Technology
School of Applied Physics
University Kebangsaan Malaysia
Bangi, Selangor 43600, Malaysia

The ORCID identification number(s) for the author(s) of this article can be found under https://doi.org/10.1002/smll.202007840.

DOI: 10.1002/smll.202007840

© 2021 Wiley-VCH GmbH

techniques such as microfiltration, ultrafiltration, nanofiltration, and reverse osmosis, ion exchange, ozonation, ultraviolet (UV) irradiation, sonodegradation, and adsorption.[19–22] Solar evaporation for water regeneration from wastewater is another technology that has been investigated for a long time but is gaining increasing attention due to novel materials being developed to increase photothermal efficiency.[23] Among these techniques, emphasis is laid on adsorption owing to its workability or ease of operation, high efficiency for pollutant removal, low cost of several adsorbents and the regeneration and reusability of some adsorbents.[19,22,24]

Numerous types of adsorbents such as activated carbon,[25,26] agricultural residues,[27,28] natural and synthetic polymers and their composites[29,30] have been used for the removal of pollutants from water and wastewater. There are many comprehensive reviews which have discussed a wide number of classes and categories of these adsorbent materials.[31–35] Although these adsorbents provide high elimination efficiencies, most display low selectivity and adsorption capacities, limiting their practical use to remove pollutants. Typical adsorbents have a number of weaknesses and do not yield the required pollutant removal effectiveness. Therefore, there is a need to design smart adsorbents which have the ability to take up pollutants present in low concentrations at a high adsorption capacity.

A key question to ask is "why are smart and selective adsorbents better than adsorbents which have been fabricated before?" Smart and selective adsorbents, as a novel breed of materials, are unique because they are tunable[36] and/or have reversible physical and chemical attributes such as selectivity,[37,38] porosity,[39,40] swelling behaviors,[41–43] thermostability,[42,44] reusability,[45] magnetic properties,[46,47] and electronic properties.[48] These properties can be harnessed prudently for controlling the various environmental parameters involved in separation or adsorption. The design, fabrication, characterization, and performance assessment of these smart and selective materials have unleashed a new research opening in water treatment and remediation. Nanoscience application has been quite relevant within the framework of smart adsorbent materials synthesis.[49–53] One merit of nanoscale adsorbents over conventional ones is that nanomaterials are endowed with much greater surface area-to-volume ratios[54,55] and relatively short diffusion paths,[56–58] which result in fast extraction rates and high extraction efficiency.[59] More interestingly, the potential use of these smart materials for water remediation comes with the possibility of tailored in situ control in contrast with treatment being simply effected by tuning the state of the stimulus/stimuli involved. In addition, these materials can have anti-fouling,[60–62] self-cleaning,[63–65] and self-healing[66–70] properties so that their operational life is enhanced. This can provide room to work towards lower overall process costs.

The word 'SMART' can be portrayed as an acronym of the following significant characteristics sought in a highly effective and versatile adsorbent. The 'S' for 'simple' fabrication at small (gram) scale and also at large (kilogram) scale. The 'M' for 'modifiable' properties which can impart adequate versatility to the adsorbent under variable environmental conditions of temperature, ionic strength, pH, light intensity, and effects of competing species. The 'A' for adequately 'adsorptive' towards target species. The 'R' for being 'reusable' enough to ensure multiple usage cycles, and finally the 'T' is for 'transferable'. This would connote preserving the set of favorable properties of the adsorbent observed at the lab scale and allowing them to be still expressed at larger scale in the remediation of real world contaminated aqueous media. Being SMART implies specific characteristics an adsorbent needs to embody to qualify for potential applications in remediating contaminated waters. The advantages available in an adsorbent when it is SMART are related to its ability to auto-modulate its response and performance in removing sustainably pollutant species from an aqueous media. Sustainable includes the following capabilities: its ability to self-control its uptake capacity for target species, its ability to be regenerated up to a certain realistic number of adsorption/desorption cycles, and its ability to be transferred from one aqueous environment to another and still maintain its high adsorption performances.

All of what is said above motivates probing deeper into the major types and performances of these advanced materials. With these observations in mind, this review compiles and analyzes the salient features, potentials, and sequestration performances of stimuli-responsive and highly selective adsorbents for metal ions and xenobiotics. The selectivity, reusability, self-healing, and self-cleaning characteristics of smart adsorbents are also discussed. Finally, the research gaps and certain key propositions for future research and development directions in relation to smart adsorbents are discussed.

2. Stimulus-Responsive Adsorbents

Outstanding performance and incomparable efficiency signifies the role of smart materials in water decontamination. Stimuli-responsive materials, with a controlled and adjustable single-stimulus (such as temperature, pH, and light) and multi-stimuli systems (two or more stimuli applied simultaneously or in turn in an advantageous targeted manner) are in booming demand. Included are the stimuli-responsive adsorbents (switchable functional materials), fabricated with tailor made properties, which upon stimulation display markedly different properties with reversible mechanisms. Both the external (including heat, light, mechanical force, pressure, and electromagnetic field) and internal (including pH, guest molecule, redox behavior, and ionic strength) stimuli can manipulate their properties. For example, ionic strength-responsive zwitterionic copolymer hydrogels were fabricated via free radical copolymerization of sulfobetaine methacrylate (SBMA), with other functional monomers, namely, sodium p-styrene sulfonate (NaSS), acrylic acid (AA), *N*-isopropylacrylamide (NIPAM) and 2-(dimethylamino) ethyl methacrylate (DMAEMA).[71] The synthesized hydrogels showed swelling behavior, and the PSBMA and PSBMA-NaSS hydrogels exhibited ionic strength sensitivity, while controlled swelling behavior with change in ionic strength was observed for PSBMA-NaSS hydrogel.[71] Increasing ionic strength (0.1–1.0 mol kg^{-1}) significantly improved MB uptake on NaSS (77–215 mg g^{-1}) and PSBMA-NaSS hydrogel (37–364 mg g^{-1}). Due to an increase in the ionic strength, the salts ions weakened the repulsive interaction of negatively charged groups present over NaSS surface. On the other hand, the electrostatic attraction between positively and negatively charged groups of PSBMA

© 2021 Wiley-VCH GmbH

was also weakened by salt, consequently improving MB uptake on both NaSS and PSBMA with increase in ionic strength.[71]

A reported redox-responsive metal-organic hybrid gel (owing to the presence of Cu^+ metal centers throughout its structural backbone) was synthesized by a reaction between 2-mercaptobenimidazole (2-MBIm) and copper(II) chloride in alcoholic medium.[72] During the synthesis, 2-MBIm reduces Cu^{2+} to Cu^+. The formation of a freeze-dried gel was triggered through Cu(I)-ligand coordination and extensive hydrogen bonding interactions involving the "−NH" protons, solvent molecules, and chloride (Cl^-) ions.[72] This freeze-dried gel was tested for hexavalent chromium (Cr^{6+}) removal with ≈331 mg g^{-1} uptake at pH ≈ 2.7.[72] During adsorption, Cr^{6+} ions were trapped throughout the porous gel network and reduced to trivalent chromium ions (Cr^{3+}) through electron transfer from monovalent Cu centers, and subsequently oxidizing monovalent Cu ions to bivalent Cu ions.[72] Therefore, Cr^{6+} adsorption resulted in gel deactivation for further removal. However, treatment of the oxidized gel matrix with ascorbic acid instantaneously reduced Cu^{2+} to Cu^+ ions. Thus, this gel-matrix was reactivated for Cr^{6+} ion uptake making it a redox-switchable phenomenon.[72] Hence, adsorbent properties can be modulated without any change in their appearance through external stimuli. Internal stimuli do not require additional stimulation, but are comparatively slow and inaccurate.[73] This section discusses the different stimuli-responsive adsorbents employed so far in water purification applications.

2.1. Single Stimulus-Responsive Adsorbents

2.1.1. Thermocontrolled Adsorbents

Thermoresponsive polymers refer to a category of materials that display varying characteristics as temperature changes.[74–77] The term is frequently employed for materials that exhibit hydrophilic/hydrophobic properties (amphiphiles) as a response to temperature changes. Thermoresponsive polymers may be classified into lower critical solution temperature (LCST) polymers or upper critical solution temperature (UCST) polymers.[77,78] LCST polymers are soluble below the LCST, but their solubility is reduced as the temperature rises above this transition temperature, must be replaced by UCST polymers are insoluble below the UCST but are able to dissolve as the temperature rises above this transition temperature.[77,78] Such thermoresponsive polymers have found use in several fields, including biomedical applications, bio-analysis and environmental applications.[79,80] Thermoresponsive polymers are gaining increasing interest for environmental applications as thermocontrolled adsorbents that are responsive or sensitive to temperature changes.[81–84] They are capable of selective adsorption and desorption under varying temperature conditions.

Poly(NIPAM), (PNIPAM), one of the most commonly studied thermocontrolled adsorbents, possesses the capacity to respond to temperature changes by experiencing a coil (soluble state) to a globule (insoluble state) phase transition when the temperature is raised above its LCST (≈32–34 °C).[52,85–89] The hydrophilicity of PNIPAM below the LCST is due to its exposed amide groups, while its hydrophobicity above the LCST is attributed to the exposed isopropyl groups and the 'hidden' amide groups.[78,87,88,90] Below the LCST, PNIPAM may form hydrogen bonds with water molecules, thereby making it soluble, while its insolubility above the LCST is due to the instability and loss of hydrogen-bonding with water molecules.[91,92] Above its LCST, the flocs are formed due to the hydrophobicity, allows the contaminants to be precipitated from solution.[93–95] PNIPAM's change in hydrophilic/hydrophobic properties and varying binding abilities with its surface allows adsorption and desorption to be conducted using temperature as a controllable trigger.[87,96,97]

The hydrophilic/hydrophobic reversible thermoresponsive characteristic of PNIPAM makes it a smart adsorbent for removal of toxic pollutants such as organic compounds and metal ions. However, to ameliorate the adsorbent efficacy, PNIPAM has been modified or mixed with other materials. For instance, PNIPAM was co-polymerized with butyl acrylate for adsorption of pentachlorophenol. The removal of pentachlorophenol was much higher for PNIPAM-11% butyl acrylate hydrogel (81%) as opposed to that for pure PNIPAM hydrogel (50%).[98] The authors also reported that the thermoresponsive nature of PNIPAM allowed the desorption of the pentachlorophenol above the LCST of PNIPAM, while a subsequent lowering of the temperature (below the LCST) caused the PNIPAM hydrogel to be regenerated and reused for further adsorption.[98] Diazinon and chlorpyrifos removal using NIPAM copolymerized with 3-allyloxy-1,2-propanediol was assessed at pH (5–9), contact times (1–30 min), and initial contaminant concentrations (25–150 mg L^{-1}).[92] Maximum contaminant removal was observed under neutral pH conditions whilst uptake improved at low initial concentrations and higher contact times.[92] The authors also reported that maximum adsorption occurred under the LCST, at a temperature range of 20–25 °C, owing to the higher solubility of NIPAM and its expanded form, thereby providing more active sites for adsorption.[92]

Nanocomposites are another way to employ PNIPAM for adsorption. For instance, powdered activated carbon (PAC) was grafted with PNIPAM for removal of bisphenol A (BPA). Self-flocculation of the hybrid composite adsorbent occurred when heating to 40 °C (>LCST of PNIPAM ≈ 32 °C), thereby adsorbing BPA from the solution.[93] Lowering the temperature (below the LCST) resolublizes the hybrid composite, thereby allowing reuse of the adsorbent.[93] Likewise, the synthesis and performance of another composite adsorbent (PNIPAM/Magnetite/Zeolite (PMZ)) was evaluated to sequester cesium ions (Cs^+) from water (**Figure 1**A,B). Compared to magnetite/zeolite composite and zeolite adsorbents, the Cs^+ uptake rate of PMZ was significantly higher, although the amount of Cs^+ adsorbed was almost similar for the three composite adsorbents, as depicted in Figure 1C.[95] The hydrophobic nature of the PNIPAM above the LCST (32 °C) resulted in the aggregation and flocculation of PMZ particles, thereby assisting in the removal of the adsorbed Cs^+ from solution.[95]

In another study, a thermo-stimuli-responsive adsorbent (TRP@MS) incorporated thermo-responsive PNIPAM into the pores of a mesoporous silica (MS) matrix.[99] Therein, maximum coomassie brilliant blue (CBB) (23.8 mg g^{-1}) and MB (22.5 mg g^{-1}) uptake by the TRP@MS was observed above the LCST (>45 °C).[99] Desorption of dye molecules at 25 °C was

© 2021 Wiley-VCH GmbH

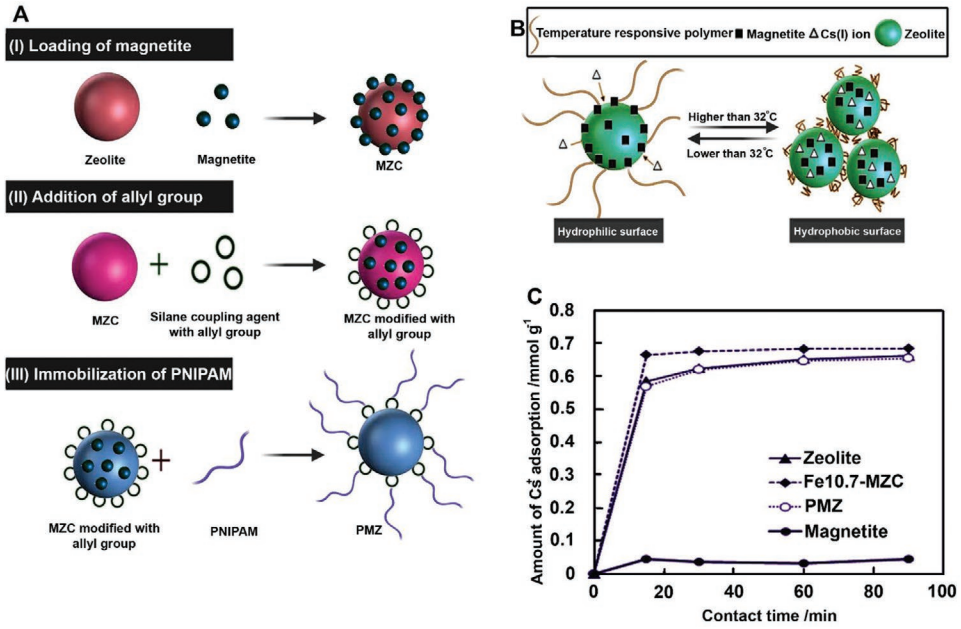

Figure 1. A) Schematic illustration of MZC, magnetite-zeolite composites; PNIPAM, poly(N-isopropylacrylamide); PMZ: MZC modified with poly(N-isopropylacrylamide) fabrication of thermoresponsive polymer/magnetite/zeolite composite adsorbent, B) Cs^+ adsorption and PMZ flocculation with changing temperatures, and C) Comparative adsorption of Cs^+ using the thermoresponsive polymer/magnetite/zeolite composite adsorbent as opposed to the other adsorbents. Reproduced with permission.[95] Copyright 2017, Elsevier.

30%, while 100% desorption was observed at 45 °C.[99] Another novel thermo-responsive polymer with selective adsorption and energy saving regeneration characteristics was synthesized via grafting PNIPAM on MS (TP@SBA-15).[81] The adsorption capacities of Neutral Red (NR, molecular size: 10.9 × 6.2 Å), and Basic Violet 4 (BV, molecular size: 16.5 × 14.6 Å) dyes on TP@SBA-15 at 25 °C (<LCST) were found to be 22.3 and 11.9 mg g^{-1}, respectively versus 23.7 and 27.5 mg g^{-1} at 45 °C (>LCST), respectively.[81] Desorption of NR from saturated TP@SBA-15 was 43% at 25°C and 95% at 45 °C with no evident decrease in adsorption capacity after five consecutive regeneration cycles.[81]

Several studies have investigated the impact of temperature on heavy metals and other contaminants removal capacity and desorption rate using a thermoresponsive polymer. For example, the effectiveness of employing an imprinted polymer prepared from 4-vinylpyridine and NIPAM was evaluated for the adsorption of BPA.[87] An increase in temperature below the LCST marginally enhanced the BPA adsorption capacity, while a further temperature increase (above the LCST to 50 °C) decreased the adsorption capacity.[87] This agrees with a previous report on maximum Sr^{2+} adsorption at a temperature near the LCST.[100] Likewise, an evaluation of the temperature effect on phenol adsorption using NIPAM found that adsorption increased to a maximum at 35 °C (near the LCST of NIPAM) but decreased upon a further rise in temperature.[101] The adsorption rate of MB and Pb^{2+} on an adsorbent synthesized with PNIPAM on cellulose filaments was faster at 25 °C (lower than the LCST of PNIPAM) while desorption of MB and Pb^{2+} occurred at 45 °C.[102] The increase in adsorption, up to the LCST, is attributed to the expanded form of NIPAM which provides more active sites for adsorption. The reduced adsorption above the LCST is due to contraction of NIPAM, which reduces the count of active sites for adsorption.[87,102]

A PNIPAM/magnetite composite-based adsorbent was evaluated for Cr^{3+} remediation. The adsorption of Cr^{3+} improved with increasing temperature from 25 to 50 °C, while cooling to 25 °C resulted in the release of the metal ion.[86] Increased Cu^{2+} uptake with rise in temperature was also confirmed for a composite made from immobilized magnetite nanoparticle (NP) onto PNIPAM-*co*-AA .[52] AA was reported to increase the hydrophilicity of the polymer compared to pure PNIPAM.[52] 60 °C is below the LCST of the PNIPAM-co-AA, and this explains why adsorption increased with increasing temperature as the LCST was not yet achieved.[52] This agrees with the report that Cu^{2+} adsorption and removal significantly improved at 50 °C as opposed to lower temperatures ranging from 32 to 42 °C.[94] This may be due to the higher LCST temperature of the copolymer PNIPAM/alginate compared to pure PNIPAM because of the presence of the more hydrophilic alginate,[94] a finding corroborated in a previous study.[103] Studies pertaining to the use of PNIPAM for improving adsorption of contaminants from aqueous solutions are summarized in **Table 1**.

Other thermoresponsive adsorbents have been studied in literature. The thermosensitive polymer *N*-vinylcaprolactam was employed with *β*-cyclodextrin and magnetite NPs for adsorption of fenitrothion.[104] The adsorption capacity and removal efficiency in real waste samples reached to 30 mg g^{-1} and >99%, respectively.[104] The authors also reported that maximum adsorption occurred at a temperature of 25 °C, while temperatures between 30 to 45 °C decreased the adsorption efficiency, thereby confirming the thermoresponsive nature of *N*-vinylcaprolactam.[104] Another thermoresponsive copolymer, poly(ethylene glycol)-methacrylate, was studied for removal of Cr^{6+}. The highest retention of the contaminant

 © 2021 Wiley-VCH GmbH

Table 1. Summary of selected SMART thermo-responsive adsorbents for water decontamination.

Contaminant	Adsorbent	Experimental conditions	Adsorption capacity [mg g^{-1}]	Remark	Ref.
Bisphenol A (BPA)	Powdered activated carbon (PAC)/ *N*-isopropylacrylamide (NIPAM)	Polymerization time: 5 min pH: 7.0 *T*: 25 °C	247.5	Desorption occurred as the temperature was increased to 40 °C (above the Lower critical solution temperature (LCST) of 32 °C of NIPAM) due to the hydrophobicity of NIPAM and the agglomeration and flocculation of the composite adsorbent.	[93]
Cu^{2+}	Poly (vinyl alcohol)/poly (acrylamide-co-NIPAM)	pH: 6.0 *T*: 25 °C Polyacrylamide content: 0.9 mol%	126.0	Maximum adsorption occurred at pH 6.0 (pH also a stimulus). Increase in temperature from 30 to 55 °C results a decrease in adsorption. A low temperature of 20 °C (<LCST) was thus chosen as the optimum temperature for adsorption.	[106]
Cu^{2+}	NIPAM grafted on magnetic carbon microspheres	*T*: 35 °C	45.5	Adsorption was temperature-dependent and the highest uptake rate was obtained at a temperature of 35 °C. The adsorption capacity remained as high as 88.4% after five consecutive regeneration cycles.	[107]
Cu^{2+}	NIPAM and bacterial cellulose	*T*: 45 °C	95.2	Maximum adsorption capacity occurred at a temperature of 45 °C (>LCST). Desorption rate was 98.8% and occurred by washing with water at 20 °C (<LCST). Adsorption capacity and desorption rate remained as high as 91 mg g^{-1} and 97% respectively after five cycles.	[108]
Pb^{2+}	poly (N-isopropylacrylamide) (PNIPAM) grafted on cellulose filaments	pH: 6.0 *T*: 25 °C	42.5	Maximum adsorption occurred at 25 °C (<LCST) due to higher number of active sites for adsorption and thereafter decreased with increasing temperatures. 20% of adsorbed Pb^{2+} was desorbed at a temperature >45 °C.	[102]
Pb^{2+}	NIPAM/Acrylic acid (AA)/ cellulose filament	pH: 6.0 *T*: 20 °C	80.8	Maximum adsorption occurred at 20 °C (<LCST) due to higher number of active sites for adsorption and thereafter decreased with increasing temperatures to 60 °C due to lower number of active sites for adsorption. Adsorption and desorption were also pH-dependent. Desorption occurred at pH 3.0.	[109]
Li^{+}	NIPAM-co-methacryloyloxymethyl-12-crown-4	Adsorbent dose: 100 mg *T*: 25 °C	1.4	The adsorbent was subjected to a volume phase transition from being swollen at 25 °C to becoming shrunken at 50 °C, thereby possessing lower active sites for adsorption at higher temperatures. Li^{+} adsorption efficiency was 89% with high selectivity among other metal ions.	[110]
U^{6+}	NIPAM/AA with carboxymethyl cellulose	pH: 6.0 *T*: 25 °C Initial U^{6+} concentration: 5 mg L^{-1} Adsorbent dose: 10 mg	14.7	Adsorption was temperature-dependent and was higher at a temperature of 25 °C as opposed to a temperature of 35 °C. Maximum adsorption occurred at pH 6.0 (adsorption was also pH-dependent). Maximum desorption occurred at 50 °C.	[111]
MB	PNIPAM grafted on cellulose filaments	pH: 7.0 *T*: 25 °C	37.0	Maximum adsorption occurred at 25 °C (<LCST) due to higher number of active sites for adsorption and thereafter decreased with increasing temperatures. 5–8% of adsorbed MB was desorbed at a temperature >45 °C.	[102]

occurred above the LCST of the adsorbent.[105] Nevertheless, the studies of these thermoresponsive adsorbents are rather scanty in literature and warrant further investigations.

Based on some of the aforementioned studies, for some copolymers involving PNIPAM, the LCST is much higher than that of pure PNIPAM (32–34 °C). Here, the adsorption keeps on increasing with increasing temperatures (beyond the LCST of pure PNIPAM). However, this increasing adsorption also implies an increase in the energy requirement of the treatment process and an increase in the cost of wastewater treatment. For lab-scale experimentation, this may not be significant. However, for large-scale implementation of the technique, the higher costs associated with the higher energy demand due to increasing temperatures may imply that the increased adsorption is not warranted. In this context, it is recommended that further studies on the use of NIPAM as a thermocontrolled adsorbent must focus on lab-scale experiments and also extend to pilot scale studies. The technical and economic viability of implementing such a technique on large scale must be prioritized.

© 2021 Wiley-VCH GmbH

2.1.2. Photo-Regulated Adsorbents

Adsorption is an interfacial phenomenon that consecutively involves the occurrence of adsorbate uptake and adsorbent regeneration. Usually, practical efficacy of the process can be enhanced if the adsorbents are responsive to external stimuli and shelter or show their active sites on demand.[36,112] Today, introducing a novel class of adsorbents that have both selective uptake and efficient recovery is extremely important.[113] Recently, studies on photo-regulated materials (examples in **Table 2**) have been widely carried out since light as an external stimulus has distinctive gains compared to other classes of stimulus.[114] The switchable molecular behavior can be organized through light remotely and applied/removed rapidly. Moreover, light can be transported to a central position specifically. Consequently, photo-regulated materials employed in several areas have been studied.[115–117] In general, light-responsive (or photo-responsive) adsorbent materials, typically among frameworks, such as metal–organic frameworks (MOFs)[118,119] and porous aromatic frameworks (PAFs),[120,121] are fabricated by combining photo-responsive components including azobenzene (AZ), stilbene, spiropyran, fulgide, and diarylethene into their matrices.[122] These photo-responsive components can be used as surface pendant groups, guest molecules or backbone of organic linkers of adsorbent materials.[123–126]

Azobenzenes (AZs) can reversibly transform between *cis* and *trans* isomerization by stimulation with ultraviolet (UV)- and visible light.[127–129] Therefore, AZs are the promising candidates which can shelter and expose active sites to adsorbates in a way which is well adjusted through ultraviolet-visible irradiation on demand.[130–132] It is noteworthy that this objective could be achieved through supports with appropriate pore sizes. Macro-and meso-porous materials possess favorable porosities; consequently, both large and small adsorbate molecules can migrate through the pore channels and reach the active sites, resulting in the selective adsorption failure.[133–135] Among them, mesoporous materials (with pore sizes between 2 and 5 nm) are highly effective in catching adsorbate molecules irrespective of their size.[36] For example, a photo-responsive adsorbent was constructed by embedding a photo responsive molecule, 4-(3-triethoxysilylpropylureido)azobenzene, onto mesoporous silica (MS) pores followed by MB and brilliant blue (BB) abatement from aqueous solutions (**Figure 2**A).[136] The AZ derivatives are employed as the molecular gates of mesopores. These gates are reversibly opened and shut off through photo-stimulation. Visible light radiations isomerize AB molecules from *cis* to *trans* configuration, resulting in partial blockage of the pore orifices (Figure 2B). MB and BB adsorption behaviour onto AZ-functionalized MS showed that for the small molecule MB, exposure to UV light has no appreciable effect on uptake. (Figure 2C). Nevertheless, for the large molecule BB, exposure to UV light results in a sharp rise (of 86.4%) in BB uptake (Figure 2D). This leads to a high selectivity for MB over BB on AZ-functionalized MS after irradiation, which is much higher than before irradiation. The density of AZ molecular is significantly impacts adsorption with an optimum AZ loading of 8.7 wt% (Figure 2E).

Another smart photo-responsive adsorbent was fabricated by introducing AZ derivatives with *cis*/*trans* isomers to Ce-doped MS for MB and BB removal.[36] The AZ groups assists as molecular switches through covering and revealing active sites, which results in effective removal and regeneration processes. Ce was doped to supply further active sites for improving adsorption performance. The *cis* isomers efficiently cover the active sites, resulting in selective MB adsorption compared to BB, whereas the *trans* isomers fully reveal the active sites, and subsequently lead to the suitable release of the adsorbates.

4-(3-triethoxysilylpropyl-ureido)-azobenzene (AZ-TPI) was introduced as a photo-stimulus responsive molecular switch into the pores of a MS namely MCM-41, and used to adsorb/desorb neutral red (NR) (molecular diameter 0.92 nm) and coomassie brilliant blue (CBB) (molecular diameter 1.91 nm) dyes from water.[113] Reversible *trans-cis* isomerization of the azo bond (present AZ) was induced by irradiation with UV (365 nm) and visible light, respectively. UV light turned on the molecular switches through photo-isomerization to the *cis*-configuration offering additional room for guest molecules but obstructing the active sites (silanol groups on the internal MS surface) so only small NR molecules can travel through the minimum gaps between the active sites and the molecular switches. Since the CBB molecules entrance is impeded, this photo-isomerization resulted in selective adsorption, and exposure to visible light reversibly turned off molecular switches changing it from *cis* to *trans* isomers. This made CBB adsorption possible while not affecting that of NR.[113] The authors also studied NR desorption from saturated azobenzene-modified mesoporous silica (AM-3) (with 17.3 wt% AZ-TPI content) which was found to be 95.6% when the molecular switch was in *trans* configuration, while just 74.9% of NR was recovered in the *cis* configuration.

Guan et al.[137] developed SP@Fe_3O_4 and SP@SW, using photo-switchable spiropyran (SP) featuring indole and benzopyran moieties conjoint at the spiro sp^3-hydridized carbon atom leading to a perpendicular orientation of both planar heterocyclic rings. During synthesis, the SP derivative was covalently immobilized onto solid spherical magnetite, Fe_3O_4, particles and the amine-functionalized planar silicon wafer (SW) surface by carbodiimide/*N*-hydroxysuccinimide mediated coupling to form SP@Fe_3O_4 and SP@SW for aqueous Cr^{3+} adsorption and desorption.[137] In the dark, the adsorption capacities of Cr^{3+} (C_o: 20 mg L^{-1}) on SP@Fe_3O_4 and SP@SW were 1.54 mg g^{-1} and 0.88 g m^{-2}, respectively.[137] The residual Cr^{3+} on the exhausted SP@Fe_3O_4 and SP@SW upon exposure to visible-light was 0.49 mg g^{-1} (68% Cr^{3+} desorption) and 0.61 g m^{-2} (30% Cr^{3+} desorption), respectively.[137] Binding potential of SP@Fe_3O_4 was tested for metal ions with different valence states. Results revealed that relatively larger amounts of trivalent metal ions were released from the SP@Fe_3O_4 surface upon exposure to visible-light, indicating efficient light-driven adsorbent regeneration with moderately stable complex formation.[137]

A photo-responsive nanoporous liquid crystal polymer film was constructed through incorporation of an AZ cross-linker in a smectic liquid crystalline hydrogen-bonded polymer network and subsequently used for treatment with an alkaline solution.[138] A polymer film exposure to UV radiation results in a reduction in smectic layer spacing, due to the shrinking of pores. Furthermore, the binding sites in the polymer film could be altered with light, leading to light-induced adsorption of cationic species.

© 2021 Wiley-VCH GmbH

Table 2. Summary of selected SMART photo- and pH-responsive adsorbents for water decontamination.

Adsorbent	Type of stimulant	Contaminant	Experimental conditions	Adsorption capacity [mg g^{-1}]	Remark	Ref.
Nanoporous polymer based on 4,4-bis(6-methacryloyloxyhexyloxy)azobenzene	Photo	Methylene blue (MB)	UV light for 180 min	N.r	Upon exposure to UV light, there was a decrease in the smectic layer spacing, and it suggested a decrease in pore size. Binding sites in the material could be varied with light, thus resulting in light-induced adsorption of cationic dyes and cations.	[138]
Modified MS with 4-(3-triethoxysilylpropylureido) azobenzene	Photo	MB and brilliant blue (BB)	UV light for 120 min	30.7 and 18.9	Irradiation with visible light at 450 nm lead to the isomerization of AB molecules from the *cis* to *trans* configuration, and the molecular gates were closed. Upon irradiation with UV light at 365nm, the AB molecules were converted from *trans* to *cis* isomers, thus aiding desorption of adsorbates because of opened molecular gates.	[136]
AB linked to MS	Photo	Neutral red (NR) and BB	UV light for 120 min	20 and 8.29	High sensitivity in reversible *trans-cis* photo-isomerization upon light-stimuli was observed in 4-(3-triethoxysilylpropylureido) azobenzene. UV irradiation led to the decrease of absorbance at 360 nm as well as an increase at 450 nm, suggesting photo-isomerization of AB linked to MS from the *trans to cis* configuration.	[113]
Graphene oxide (GO)/nanoscale zero-valent iron composite	pH	Tetracyclines	pH > 9; *T*: 25 °C; *t*: 30 min	100	Adsorption was rapid and significantly efficient even in high salty and humic acid with water under acidic to neutral conditions. At pH > 9, g GO/nanoscale zero-valent iron composite disassembled partly with increasing pH values, resulting in the elution of antibiotics for efficient antibiotics degradation by ozonization.	[147]
Magnetic borate-MOF@PDA	pH	Luteolin (LTL)	pH:8; *T*: 25 °C; *t*: 360 min	91.23	Adsorptive capacity of fresh LTL was 27.32 mg g^{-1}, and the result decreased only 6.32% after six cycles in comparison with the initial value.	[155]
Amine functionalized mesoporous SBA-15 silica	pH	Bromothymol blue (BTB) and MG	pH 7 and pH < 4; T: 25 °C	13.7 and N.r.	In a solution comprising BTB and malachite green (MG) in equal concentration, only BTB anions had been adsorbed onto the substrate for pH decreasing at values < 4.	[156]
Ammonium-functionalized based on hollow poly(maleic anhydride-*alt*-styrene)	pH	Acidic methyl blue dyes (a-MB)	pH 2; *T*: 25 °C; *t*: 600 min	200	Ammonium and carboxyl groups were found on the adsorbent exhibited a noteworthy pH-dependent equilibrium adsorption capacity, which rose significantly from 59 mg g^{-1} to 449 mg g^{-1} when pH fell from 9 to 2.	[144]
Magnetic GO/poly(*N*-vinylimidazole-*co*-acrylic acid)	pH	Methyl violet (MV), MB, tartrazine and amaranth	pH 12, 12, and 3,3; *T*: 30 °C; *t*: 120 min	609.8, 625.0, 613.5, and 609.8	Desorption of cationic and anionic dyes was performed at pH 2 and pH 12, respectively. Formation of free imidazole–N and carboxylic acid was favorable for release of anionic and cationic dyes, respectively.	[142]
Cross-linked poly(dimethylaminoethyl methacrylate)	pH	Reactive red 24 (RR 24) and fuchsin basic (FB)	pH 1.5 and 9; *T*: 30 °C; *t*: 400 min	1871.23 and 482.54	Excellent adsorption capacities for RR24 resulted from the introduction of phytic acid groups, which promoted protonation of tertiary amine groups under acidic conditions.	[145]
Cross-linked chitosan hydrogel	pH	Acid Orange 7 (AO7)	pH 5; *T*: 25 °C; *t*: 30 min	1670	AO7 adsorbed onto the microbeads at pH 5, and could be desorbed at pH 9. Asorption proceeded via electrostatic interactions occurring between positive groups of the protonized chitosan gel microbeads ($-NH_3^+$) and negative groups of the AO7 molecules ($-SO_3^-$) under acidic pH conditions.	[146]

Nr, Not reported.

© 2021 Wiley-VCH GmbH

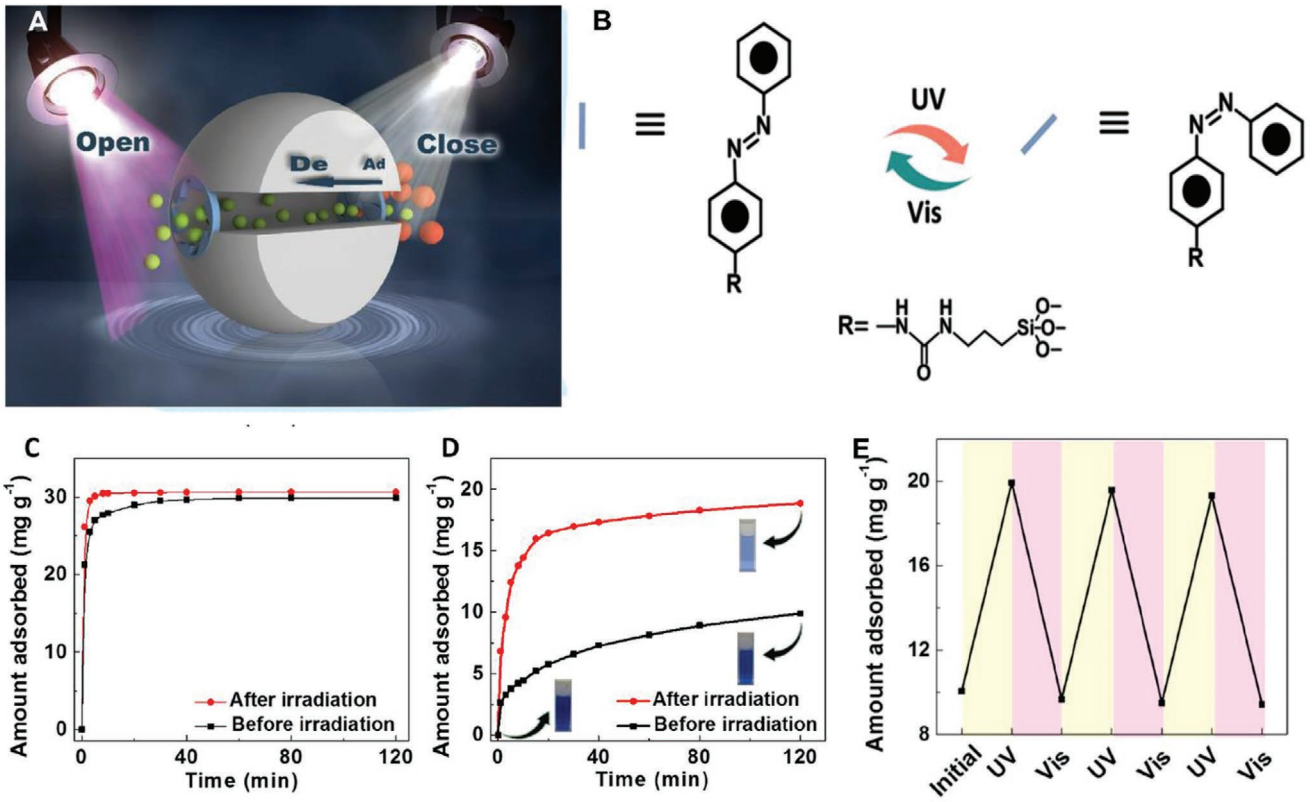

Figure 2. A) Graphic illustration of the adsorption/desorption process of a photo-regulated adsorbent which opened and closed upon light irradiation, B) Graphic illustration of molecular gates reversibly closed/opened because of photo-isomerization of azobenzene, C) methylene blue (MB) and D) brilliant blue (BB) adsorption curves on azobenzene (AZ)-functionalized mesoporous silica (MS) with and without UV light irradiation. Profiles for the initial BB solution before and after adsorption by AZ-functionalized MS is inserted in D) in the presence or absence of irradiation, and E) adsorption/desorption cycles of BB over AZ-functionalized MS (the amount of AZ is 8.7%) under UV light and visible light irradiation; The BB adsorption over the adsorbent was first operated. After saturation, desorption was completed in ethanol for adequate time to release all adsorbed dyes. Reproduced with permission.[136] Copyright 2016, American Chemical Society.

2.1.3. pH Responsive Adsorbents

The pH-responsive adsorbents (examples in Table 2) respond to the changes in medium pH *via* altering their dimensions. These adsorbents may swell or collapse depending on pH and their functional groups.[139,140] These smart materials can be classified into two categories, those with acidic (e.g. $-COOH$, $-SO_3H$, $-B(OH)_2$, $-PO_3H_2$) and basic (e.g. $-NH_2$) groups.[122,139] The response mechanism is similar for acidic and basic adsorbents, whilst only the stimulus differs. Most of the synthetic polymers (e.g. poly(acrylic acid), poly(acrylamide) polyaniline, etc.) and natural polymers (e.g. hyaluronic acid, cellulose, dextrin, dextran, chitosan, etc. and polymer gums) containing pH sensitive groups and their nanocomposites are pH responsive materials that can be used for water purification.[141–147]

pH-responsive adsorbents can be used for selective pollutant removal. For example, ammonium-functionalized hollow polymer particles (HPP-NH_3^+), with high density ammonium groups in the shell, were assessed for acidic methyl blue dyes (a-MB) removal (**Figure 3**A,B).[144] The existence of ammonium and carboxyl groups in the HPP-NH_3^+ displayed an important pH-dependent adsorption, which dramatically increased from 59 to 449 mg g^{-1} as the basic solution pH (pH 9) tends towards acidity (pH 2) (Figure 3C).[144] The a-MB saturated HPP-NH_3^+ can be regenerated at basic pH (pH10) to recover both a-MB and the HPP-NH_3^+ with high desorption efficiency (>95%).[144] In a similar work, HPP-NH_3^+, with ammonium and carboxyl functionalities in the copolymer backbone, was employed as a dual-functionalized pH responsive adsorbent to sequester basic methyl blue dyes (b-MB).[140] The b-MB adsorption capacity was reduced significantly from 516.1 to 24 mg g^{-1} by tuning solution pH (from 12 to 3). Consequently, the b-MB-adsorbed on HPP-NH_3^+ could be instantly recovered under acidic condition (pH 3) with excellent desorption efficiency (≈95%, in 30 min).[140]

There are several papers in literature reporting the use of pH sensitive copolymers and composites based on natural polymers for removal of pollutants from water. Guar gum-based hydrogel containing $-NH_2$ and $-COOH$ groups were synthesized from guar gum and polyacrylamide *via* simultaneous polymerization and crosslinking, and employed for the removal of cationic dyes viz. azure B (AB) and crystal violet (CV).[141] The AB and CV adsorption occurred because of electrostatic interaction between the oppositely charged AB and CV molecules and guar gum-based hydrogel system. About 85 and 50% AB and CV were respectively released during desorption in NaCl solution. Furthermore, CV adsorbed with a higher capacity and bound stronger than AB through the guar gum-based hydrogel network.[141]

© 2021 Wiley-VCH GmbH

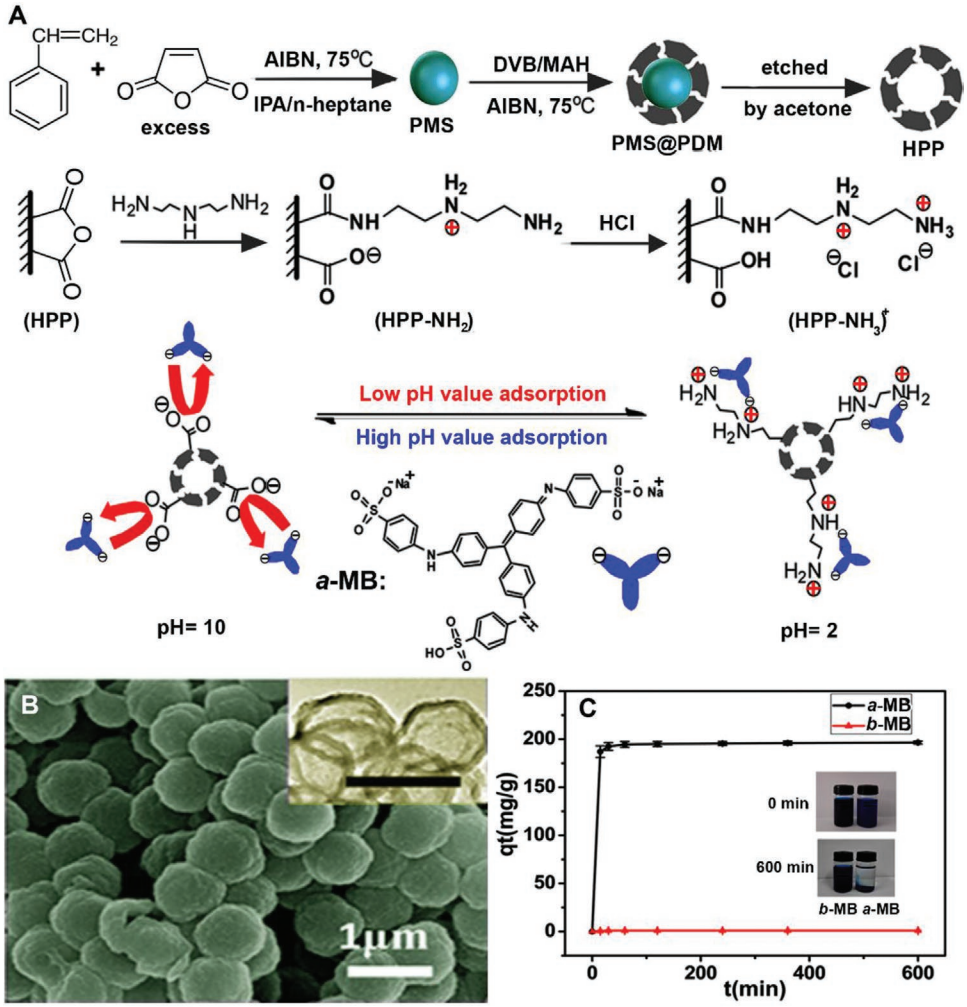

Figure 3. A) Synthesis of ammonium-functionalized hollow polymer particles (HPP-NH_3^+) and graphic illustration for the adsorption/desorption of methyl blue (a-MB) by the HPP-NH_3^+, B) SEM image of pH responsive HPP-NH_3^+, and C) effect of pH values on the adsorption of a-MB onto the HPP-NH_3^+ ($C_0 = 600$ mg L^{-1}) with the inset showing equilibrium between acidic and basic forms of the HPP-NH_3^+. AIBN: 2,2′-azobis(isobutyronitrile), DVB: divinylbenzene, MAH: maleic anhydride, PMS: poly(maleic anhydride-alt-styrene), PDM: poly(divinylbenzene-alt-maleic anhydride), IPA: Isopentyl acetate. Reproduced with permission.[144] Copyright 2016, American Chemical Society.

Carboxymethyl cellulose/graphitic-carbon nitride/zinc oxide (CMC/g-C_3N_4/ZnO) nanocomposite was fabricated by sol–gel technique for the remediation of methyl violet (MV) from aqueous solutions. Solution pH affected the adsorption rate to a large extent and maximum adsorption (96.43 mg g^{-1}) occurred at pH 8.[148] In other work, polyamine chitosan adsorbent was prepared via introduction of ethylenediamine into hydroxyl groups of chitosan for the removal of congo red (CR) and methyl orange (MO) anionic dyes from water. The maximum adsorption for both CR and MO was observed in acidic medium (pH 4). Both the amine-protected-released and the amine introduced processes increased the number of $-NH_2$ groups and resulted in an increased adsorption capacity for anionic dyes.[149]

A pH-responsive graft copolymer hydroxyethyl cellulose-graft-poly(*N*-vinyl imidazole-*co*-acrylic acid) containing both acidic and basic functionalities was fabricated for adsorption of Co^{2+}, Ni^{2+}, and $Zn^{2+}$from ternary aqueous mixtures. Metal complexation studies showed that maximum adsorption of $Ni^{2+}$and Co^{2+} ions occurred at pH 5.5 because of electrostatic attractions with carboxylate groups only, whereas Zn^{2+}ions were mostly adsorbed at pH 6.5 as a consequence of interactions with both imidazole-N and adjacent carboxylate groups. The copolymer was regenerated from the metal loaded polymer by acidic treatment. This could be explained as follows: carboxylate ($-COO^-$) and the basic nitrogen of imidazole are protonated in the presence of H^+ ions which weakens the electrostatic interaction between the metal ions and the polymer, resulting in desorption.[150]

A pH-responsive carboxymethyl cellulose/chitosan hydrogel for the removal of both anionic and cationic dyes was proposed.[152] The adsorption capacity and desorption ratio of carboxymethyl cellulose/chitosan hydrogel for acid orange II (AOII) were higher than 100 mg g^{-1} at pH 2 and 90% at pH 11, respectively. These values for MB were higher than 110 mg g^{-1} at pH 11 and 95% at pH 2 even after five consecutive

© 2021 Wiley-VCH GmbH

adsorption/desorption cycles.[151] Polyethylenimine (PEI)/ethyl cellulose (EC) composite was used as a pH-response adsorbent for removal of Cr^{6+} with a wide pH range (3–11). It was reported that 4.0 mg L^{-1} of $Cr^{6+}$from 20 mL solution was completely removed by 60 mg polyethylenimine/ethyl cellulose composite dose within a 5 min contact time under acidic conditions (pH 3). Meanwhile, 4.0 mg L^{-1} Cr^{6+} basic solutions (pH 11) can also be totally purified by 3.0 g L^{-1} (60 mg) PEI/ECs within 15 min. This shows comparatively rapid adsorption kinetics at lower pH. The introduction of PEI drastically improved the hydrophilicity of the adsorbent, which facilitates the Cr^{6+} transfer between the solid and solution phase. In addition, the amine groups present over PEI/ECs surface were protonated during the adsorption, consequently enhancing Cr^{6+}reduction to Cr^{3+}.[152]

In addition to natural polymers and their composites, other synthetic polymers and polymer-based nanocomposites such as poly(AA-*co*-methyl methacrylate), poly(dimethylaminoethyl methacrylate), polyaniline and magnetic graphene oxide (GO)/poly(*N*-vinylimidazole-*co*-AA) as pH-responsive adsorbent hydrogels have also been used to remove cationic and anionic dyes.[142,143,145] For example, the effective and pH-responsive crosslinked poly(dimethylaminoethyl methacrylate) (PAGD) adsorbent was prepared from phytic acid, glycidyl-methacrylate, and N,N-dimethylaminoethyl methacrylate (DMAEMA) was employed for adsorption of reactive red 24 (RR24) and fuchsin basic (FB) with maximum adsorption capacities 1871.23 and 482.54 mg g^{-1} at pH 3 and 9, respectively. RR24 was effectively removed by PAGD from a binary mixture of the dyes.[145] Polyaniline/sodium alginate nanocomposite was used as a pH-responsive adsorbent for the removal of orange-II (O-II) and MB from water at different pH values. The maximum adsorption of O-II (476.19 mg g^{-1}) and MB (555.5 mg g^{-1}) was reported at pH 3 and 9, respectively.[153]

A pH-responsive P4VP-NR adsorbent was prepared by free radical crosslinking of poly (4-vinylpyridine) (P4VP) and natural rubber (NRb), in the presence of benzoyl peroxide for indigo carmine (IC) dye adsorption and release.[154] A highly swollen P4VP-NRb surface was observed at pH < 4. In this pH range, pyridine, which is a weak base, converted to positively charged pyridinium salt, consequently generating electrostatic repulsion, which resulted in swelling of P4VP-NRb. At pH > 4, deprotonation of pyridine groups occurred, which led to neutral pH, resulting in less swelling. The pH-responsive behavior of P4VP-NRb was supported by contact angle measurements where a change in pH from 2 to 4 resulted in an increase of the contact angle from 28° to 80°. Maximum adsorption of the anionic IC dye on P4VP-NRb was 1.55 mg g^{-1}.[154] To study desorption capacity, IC saturated P4VP-NRb samples were immersed in aqueous solutions at various pH. Significant dye release was observed at pH 2, 8, and 10. At pH 2, the adsorbent material was highly protonated, leading to large free volume inside the material, thereby allowing IC to be released. At pH 8 and 10, vinylpyridine groups became neutral, consequently hindering interactions between P4VP-NRb and IC and thus, releasing IC dye into the aqueous solution.[154]

Functionalized MOFs and MS are also used as pH-responsive adsorbents.[155,156] The ligands that contain $-B(OH)_2$, $-OH$, $-NH_2$, $-Br$, $-NO_2$, $-SO_3$, and 5-boronobenzene-1,3-dicarboxylic acid are used to functionalize MOFs and MS.[155–160] For example, hydrophilic magnetic boric-functionalized MOF (Fe_3O_4@PDA@BA-MOFs) nanocomposites were fabricated by modifying boric acid-MOFs (BA-MOFs) onto the polydopamine (PDA)-coated magnetic microspheres, employed for the adsorption of luteolin (LTL) as a typical natural flavone.[155] Fe_3O_4@PDA@BA-MOFs pH-responsively captured LTL because of the introduction of the BA-MOFs shell. Furthermore, the pH-responsive capture and release mechanisms were based on the BA (boronic acid).[155] Indeed, at pH 8.0, the binding capacity of LTL reached its highest value, and this could be because of the introduction of BA to MOFs. In alkaline medium (pH 8) the —OH groups in BA were deprotonated, while in acidic medium (pH 5) the -OH groups were protonated and led to a release of LTL. In another study, ammonium and free amine functionalized mesoporous SBA-15 silica was used for cationic malachite green (MG) and anionic bromothymol blue (BTB) dyes removal, respectively.[156] The main reason for this behavior was the existence of strong electrostatic interaction forces or hydrogen bonding between organo-functional amine/ammonium groups and MG and BTB dyes, which was dependent on the dye species present and the media pH. Moreover, the adsorbed BTB was only recovered at pH 5 without release of MG, while MG was only recovered at pH 4 without release of BTB.[156]

2.1.4. Magnet-Responsive Adsorbents

Magnetic adsorbents are easy to separate after use, which is essential for the subsequent regeneration and reutilization, as demanded by a circular economy. In the last decades, materials that were not applicable due to separation difficulties, have become choice options following their magnetization. Such a magnetization involves surface modifications that may affect to a larger or lesser extent, the adsorptive performance of the resulting adsorbents. This will be described next. Recent advances on smart magnet-responsive composites with large efficiency, capacity and/or selectivity developed from different materials, including activated carbon (AC), polymers, graphene, zeolites, and silica, are illustrated in this section. Differently from the above single stimulus responsive adsorbents, namely thermocontrolled, photo-regulated and pH responsive, the articles reviewed on magnet-responsive adsorbents did not aim at the production and utilization of materials with an adjustable or modulated response, but just of magnetic materials that allow for their after-use simple separation by the application of a magnetic field.

Magnetic Activated Carbon: After-use recovery of powdered activated carbon (PAC) leads to material loss, negatively affecting regeneration and reusability.[161] In the search for economic feasibility, great advances have been made with the production of magnetic activated carbon (MAC) by the matrix inclusion of magnetically active components. Due to their comparatively low price, great availability, and large magnetizing capacity,[162,163] ferrites such as manganese ferrite ($MnFe_2O_4$),[164] cobalt ferrite ($CoFe_2O_4$)[165] nickel ferrite ($NiFe_2O_4$),[166] and iron oxides, namely maghemite (γ-Fe_2O_3) and, especially, magnetite (Fe_3O_4), are most commonly used.[167] Co-precipitation, either by in situ (one-step with simultaneous formation and impregnation of magnetic NPs in AC framework[168,169]) or *ex-situ* (two-step involving the synthesis of magnetic NPs followed

© 2021 Wiley-VCH GmbH

by their dispersion with AC[170,171]), are the most conventional MAC synthesis owing to their simplicity, productivity, and cost-effectiveness.[167]

Saturation magnetization (M_s) is a very important parameter when considering magnetic separation of magnetized PAC,[172] and M_s values are usually reported to support magnet responsiveness. For example, M_s of magnetite NPs is generally between 60–80 emu g^{-1} (depending on the phase purity obtained under the specific synthesis method). M_s values of MAC are usually lower due to the presence of PAC composited with these NPs but still allow for magnetic separation.[170] During magnetization, surface magnetic NPs may block pores in PAC, leading to a decrease in specific surface area (SSA),[170,173,174] which may reduce its maximum adsorption capacity. For instance, an adsorption reduction from 385 mg g^{-1} of Cr^{6+} by PAC (SSA: 936 m^2 g^{-1}, M_s: 3 emu g^{-1}) to 179 mg g^{-1} by Fe_3O_4/PAC (SSA: 464 m^2 g^{-1}, M_s: 38 emu g^{-1}).[170] However, SSA rise after magnetization has also been reported for a coconut shell based AC, with an increase from 417 to 952 m^2 g^{-1} (with increasing adsorption capacity from 20 to 24 mg g^{-1} for phenol) due to the release of micropores and mesopores previously covered by minerals that dissolved during magnetization.[175] Other authors reported average pore size increasing with Fe_3O_4 and $MnFe_2O_4$ introduction resulting in 2.8- and 2.5-fold higher glyphosate uptake onto Fe_3O_4/PAC (SSA: 694 m^2 g^{-1}, M_s: 14 emu g^{-1}) and $MnFe_2O_4$/PAC (SSA: 502 m^2 g^{-1}, M_s: 73 emu g^{-1}), respectively, than on the original PAC (SSA: 1360 m^2 g^{-1}).[174]

Other methods that have been used for the synthesis of MAC include solvothermal reduction,[176] hydrothermal treatment,[166] combustion,[177] or impregnation pyrolysis.[165] The latter has been frequently reported for alternative AC produced from biomass and biowastes, and can be carried out either as pre-coating (magnetic and carbonaceous precursors are mixed and then pyrolyzed[178,179]) or post-coating (carbonaceous precursor is pyrolyzed and then impregnated with the magnetic component[180]). For example, ferric chloride ($FeCl_3$) allowed for producing a MAC from bermudagrass with 1013 m^2 g^{-1} of SSA and 265 mg g^{-1} of sulfamethoxazole (SMX) adsorption capacity (whose magnetic separation was visually demonstrated), while the non-magnetic biochar respectively displayed 86 m^2 g^{-1} and 15 mg g^{-1}.[181]

Functionalization of MAC is a current strategy for increasing adsorptive performance. Core-shell functionalized modified MAC, namely MFMPAC and MFMWAC, were prepared by using peach stone or wood AC precursors, respectively, which were subjected to phosphoric acid modification, followed by magnetization and functionalization with ethylenediaminetetraacetic acid (EDTA).[182] MFMPAC (SSA: 458 m^2 g^{-1}, M_s: 0.12 emu g^{-1}) and MFMWAC (SSA: 415 m^2 g^{-1}Ms: 14 emu g^{-1}) respectively displayed MB adsorption as high as 438 and 434 mg g^{-1} (pH: 7, T: 298 K, C_0: 50 mg L^{-1}) in a single solution, which decreased to 183 and 175 mg g^{-1} in binary solution containing Pb^{2+}.[182] $NiFe_2O_4$ was used for the magnetization of AC (SSA: 1787 m^2 g^{-1}) to produce $NiFe_2O_4$-PAC (SSA: 1594 m^2 g^{-1}, M_s: 26 emu g^{-1}), which was then functionalized with thiol to obtain $NiFe_2O_4$-PAC-SH (SSA: 1241 m^2 g^{-1}, M_s: 21 emu g^{-1}) with 366 mg g^{-1} of Hg^{2+} adsorption capacity (pH:7, T: 298 K, C_0: 30 mg L^{-1}).[183] An AC was magnetized with both $FeCl_3$ and ferrous sulfate ($FeSO_4$) and then impregnated with Aliquat 336 (*N*-Methyl-*N,N,N*-trioctylammonium chloride), the functionalized MAC was used for BPA adsorption with a capacity of 1.6 mg g^{-1} (T: 303 K, C_0: 10–50 mg L^{-1}).[184]

In the case of organic pollutants, research has been recently directed to adsorptive-reactive removal by functionalized MAC. Reduction of Pd^{2+} onto Fe NPs already embedded within a previously produced MAC (SSA: 880 m^2 g^{-1}, M_s: 3 emu g^{-1}) doped this MAC with Pd NPs that allowed for orange II catalytic degradation.[185] In only 5 min, the functionalized MAC removed 68% of the dye, as compared with 30% and 10% by MAC and AC, respectively.[185] A facile procedure involving ethanol pre-adsorption on AC followed by addition of $NiFe_2O_4$ and silica gels and then mixing with TiO_2 NPs resulted in the production of a novel material, TMAC (M_s: 6 emu g^{-1}), targeted for tannic acid adsorption.[186] TMAC, whose SSA (909 m^2 g^{-1}) was close to that of the precursor AC (1414 m^2 g^{-1}) due to micropore preservation by pre-adsorbed ethanol, allowed, under UV irradiation, for a 99% removal in 150 min.[186] Magnetic nanocomposites (SSA: 223–333 m^2 g^{-1}, M_s: 3–14 emu g^{-1}) were innovatively synthesized by loading Ni-doped anatase TiO_2 on MAC and evaluated as dyes degrading adsorbents, with 98% removals for basic fuchsine, CV and MG in just 10 min under visible light.[187]

Some MAC studies have taken advantage of Fe_3O_4 NPs ability to activate reactive species production by oxidants (such as hydrogen peroxide, persulfate and peroxymonosulfate) thereby enhancing Fenton degradation of organic pollutants. A TiO_2 functionalized MAC (T@MPAC) was produced, characterized, and then tested for benzotriazol adsorption and photocatalysis.[188] T@MPAC (SSA: 270 m^2 g^{-1}, M_s: 25 emu g^{-1}) possessed lower SSA than the precursors MAC (SSA: 573 m^2 g^{-1}, M_s: 35 emu g^{-1}) and AC (SSA: 745 m^2 g^{-1}) but displayed comparable adsorptive performance (39% as compared with 36% (MAC) and 45% (AC); T: 298 K). After saturation, peroxymonosulfate addition and UV irradiation allowed for efficient regeneration by benzotriazol degradation (>92%).[188] A TiO_2 decorated MAC (SSA: 270 m^2 g^{-1}, M_s: 25 emu g^{-1}) coupled with UV and ultrasound irradiations was used for the adsorptive-reactive removal of tetracycline (TC).[189] Optimized TC removal was >93% after 180 min, while in the presence of oxidants, namely, hydrogen peroxide, persulfate, peroxymonosulfate, or periodate, it was complete in just 60 min.[189]

Magnetic Polymeric Adsorbents: Polymeric adsorbents have become alternatives to ACs due to their surface area, thermal stability and robustness, feasible mild regeneration and, especially, adjustable surface chemistry and pore size distribution, which result in high efficiency and selectivity. Recently, the development of magnetic polymeric smart adsorbents and their use for removing organic and inorganic pollutants have impressively increased due to their easy and simple after-use separation.

An innovative magnetic alginate/polyethyleneimine (ALG/PEI)$_n$/MN was synthesized by deposition of ALG/PEI multilayers onto amine-modified Fe_3O_4 microspheres (MN) by the layer-by-layer (LbL) methodology for acid orange 10 (AO10) adsorption.[190] The larger the number of coated (ALG/PEI) bilayers, the better the (ALG/PEI)$_n$/MN performance, displaying 246 mg g^{-1} as maximum adsorption of AO10 (T = 298 K).[190] An ionic cryogel was synthesized by crosslinking polymerization of 2-acrylamido-2-methylpropane sulfonate

© 2021 Wiley-VCH GmbH

sodium salt and styrene sulfonate sodium salt. $Fe_3O_4.Cu_2O$. Fe_3O_4 NPs evolved inside the cryogel by reduction–co-precipitation to produce magnetic Na-AMPS/SS-Na/ $Fe_3O_4.Cu_2O.Fe_3O_4$ (magnetic saturation, M_S: 12 emu g^{-1}), which displayed a MB removal capacity of 833 mg g^{-1}, maintaining magnetic characteristics and efficiency for six cycles under regeneration with methanol/ammonia.[191]

Diclofenac (DCF), atenolol (ATN) and ceftriaxone (CFX) were efficiently adsorbed from water by St-AMPS, a magnetic poly (styrene-2-acrylamido-2-methyl propanesulfonic acid) that was synthesized by mini-emulsion polymerization, using hydrophobic magnetite NPs coated with oleic acid.[192] St-AMPS (M_S: 48 emu g^{-1}) displayed adsorption capacities of 151, 48, and 120 mg g^{-1} for DCF, ATN, and CFX, respectively, with good alkaline (pH: 8) regeneration potential and reusability during four cycles.[192]

Magnetic molecularly imprinted polymers (MIPs), which are highly selective for organics thanks to their tailor-made binding sites, have become a research hotspot for pharmaceuticals removal. Quinolone selective adsorption was studied using a magnetic surface MIP (SMIP) in which magnetic carbon nanospheres (MCNSs) were the core, quinoline the template and acrylamide (AAm) was used as functional monomer.[193] The synthesis of SMIP/MCNSs (**Figure 4**A,B) involved silanisation, imprinting (grafting + crosslinking) and elution steps, the resulting optimized material (SSA: 87 m^2 g^{-1}, M_S: 22 emu g^{-1}) had a removal capacity of 131 mg g^{-1} (T: 298 K), with high selectivity (Figure 4C) and remarkable efficiency in real cooking wastewater.[193]

Magnetic yeast (MY) was produced through an in situ one-step method and served as the core for MIPs, using SMX as template, to produced core-shell MY@MIPs (SSA: 43 m^2 g^{-1}, M_S: 34 emu g^{-1}) for selective adsorption of SMX, with a maximum capacity of 77 mg g^{-1} (pH: 4, T: 298 K).[194] A novel magnetic MIP (MMIP), namely $CoFe_2O_4$@TiO_2-MMIP, combined adsorption, photocatalytic degradation and magnetic separation for norfloxacin (NOR) removal.[195] First, $CoFe_2O_4$@TiO_2 was prepared by hydrothermal reaction and then an improved liquid phase deposition with NOR as template was done to obtain $CoFe_2O_4$@TiO_2-MMIP, which displayed a removal capacity of 14 mg g^{-1} (1.8× larger than by $CoFe_2O_4$), high selectivity, and photo-catalytic regeneration ability (83% removal after nine cycles).[195]

Magnetic polymeric materials have been also successfully used for the adsorption of metal ions. A homogeneous polypyrrole film was synthesized by polymerization on the surface of a magnetic mixture of Fe_3O_4 and $FeCl_3$, resulting in a core–shell PPy/Fe_3O_4 (M_S: 14 emu g^{-1}) with an optimized Hg^{2+} uptake of 173 mg g^{-1}, and high regeneration ability (>90%).[196] A magnetic polymeric resin (EG@$CuFe_2O_4$; SSA: 226 m^2 g^{-1}, M_S: 32 emu g^{-1}) was fabricated using ethylenediaminediacetic acid, glutaraldehyde and $CuFe_2O_4$ NPs for Hg^{2+} and Pb^{2+} adsorption, with respective capacities of 270 and 215 mg g^{-1}, which decreased to 180 and 160 mg g^{-1} after seven cycles (regeneration with 0.1 M HCl).[197]

Naturally occurring polymers, among which cellulose is the most abundant followed by chitosan, have also been used for the synthesis of magnetic smart adsorbents. A 3D magnetic polymeric aerogel (MBCNF/GOPA; SSA: 215 m^2 g^{-1}, M_S: 27 emu g^{-1}), which was produced from bacterial cellulose nanofibers (BCNFs), Fe_3O_4 NPs, nanosheets of GO, and polyvinyl alcohol (PVA) by networks filler-loading combined with vacuum freeze-drying, was used for MG adsorption with a maximum capacity of 270 mg g^{-1} (pH: 7, T: 298 K), as described in **Figure 5**.[198] A composite of carboxymethyl cellulose (CMC), which has strong affinity for metal ions, and chitosan (COS) was magnetized with Fe_3O_4, freeze dried, and grafted with EDTA, an excellent metal chelator, to produce a novel Fe_3O_4@CMCCOS-EDTA (M_S: 47 emu g^{-1}) with large adsorption capacity for Pb^{2+} (432 mg g^{-1} at pH: 5, T: 308 K) and excellent stability and regeneration ability using EDTA.[199] Fe_3O_4-coated nanofibers based on cellulose acetate and COS were produced and used for Cr^{6+}, Ni^{2+} and phenol adsorption, their capacities being 193, 143, and 163 mg g^{-1} (T: 298 K), respectively, which remained >90% after five cycles.[200]

Magnetic Graphene Based Adsorbents: Graphene (GN) and GO are carbon materials with relevant properties (high SSA, chemical stability, and active surface functional groups) for adsorption applications.[201,202] However, due to their dispersibility, GN based materials are difficult to recover from water, with magnetization being a solution to enhance their implementation. In the last decade, functionalized GN magnetic composites have emerged as novel smart adsorbents. GO-gadolinium oxide (GO-Gd_2O_3; SSA: 51 m^2 g^{-1}, M_S: 55 emu g^{-1}), which was synthesized as a magnetic hollow-sphere nanocomposite, adsorbed As^{5+} through complexation or electrostatic interactions, having an adsorption capacity of 217 mg g^{-1} (pH: 6, T: 293 K) and having photocatalytic antimicrobial activity.[203]

Reduced GO (rGO) was produced by a Hummer's method and decorated with $MnFe_2O_4$ NPs by the sol-gel method, the resulting material (MRGO; SSA: 95 m^2 g^{-1}, M_s: 8.5 emu g^{-1}) having a MB uptake capacity of 105 mg g^{-1} (pH: 7.5).[204] Amphiprotic cellulose (AP-MCC) was used as a mediator for GO and Fe_3O_4 self-assembled gelation in order to produce a magnetic aerogel (MAG; M_S: 9 emu g^{-1}) that contained channels with amphiprotic surface active groups allowing for adsorption of both anionic and cationic chemicals.[205] Its adsorption capacity towards congo red (CR) and MB was 282 and 346 mg g^{-1}, while it was 222, 568, 186, and 122 mg g^{-1} respectively for Cu^{2+}, Pb^{2+}, Cd^{2+}, and Cr^{3+}, in all cases maintaining > 68% capacity at the end of five cycles. After preparing GO from graphite by the modified Hummers's method, the co-precipitation method was used to prepare MGO, which was then converted into MGO/ZnO nanocomposites (MZ). MZ (SSA: 83 m^2 g^{-1}, M_S: 11 emu g^{-1}) displayed a TC adsorption capacity as high as 1590 mg g^{-1} (pH: 6, T: 313 K), with electrostatic attraction, π-π interaction, hydrogen bonding, cation exchange, and complexation as main mechanisms. TC photocatalytic degradation by MZ was verified, with GO acting as framework and electrons transfer promoter and ZnO as photocatalyst.

A waste-based magnetic fullerene nanocomposite (FMFN) aimed at ciprofloxacin (CIP) adsorption was synthesized by the catalytic thermal decomposition of waste polyethylene terephthalate and ferrocene as a catalyst and magnetite precursor.[206] FMFN (SSA: 337 m^2 g^{-1}, M_S: 7 emu g^{-1}) provided a CIP maximum capacity of 373 mg g^{-1} (pH: 6, T: 313 K) thanks to the interaction between CIP (electron donor) and the π-electron depleted regions of FMFN surface (electron acceptor), with negligible efficiency reductions through five cycles.[206]

© 2021 Wiley-VCH GmbH

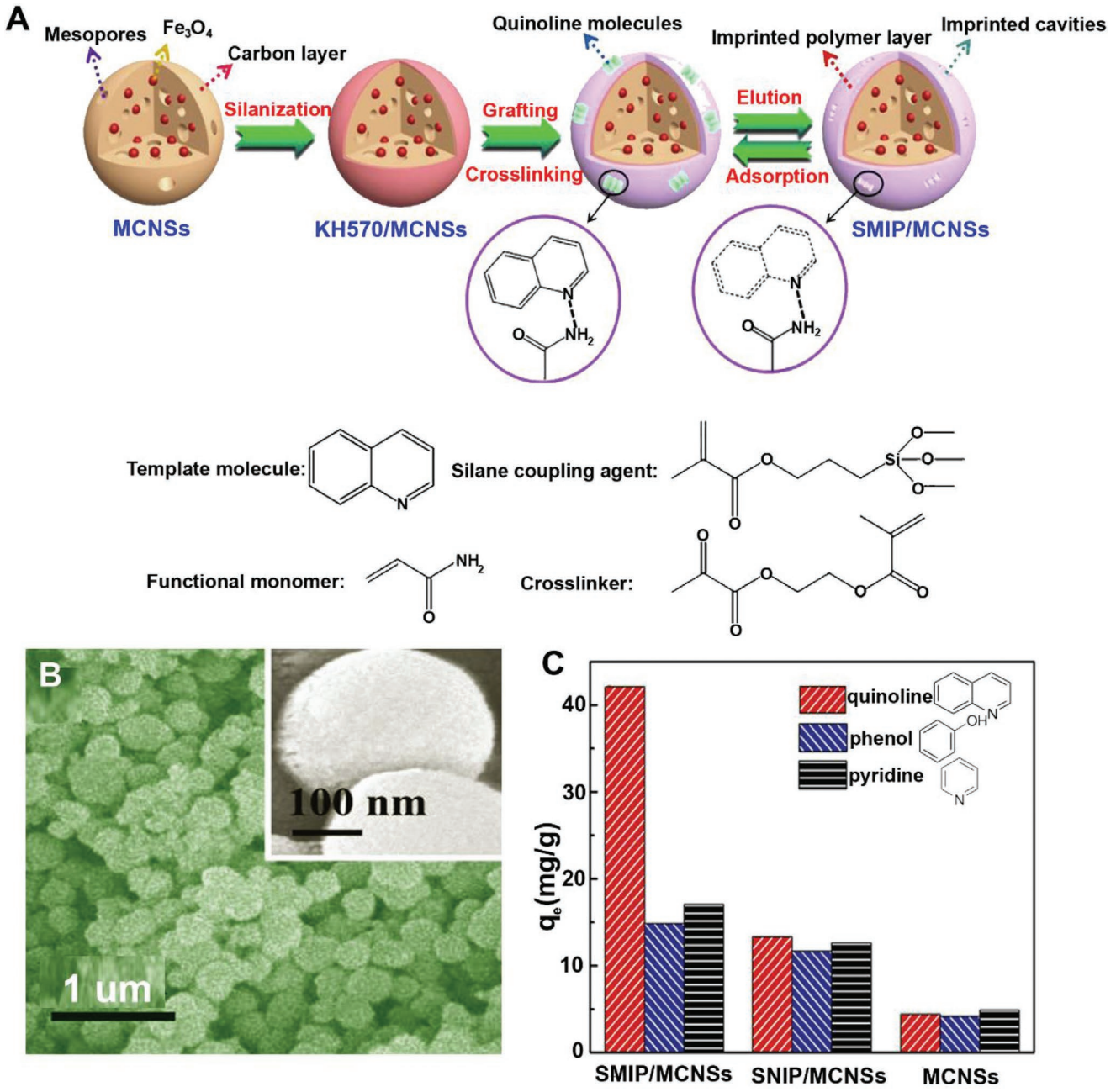

Figure 4. A) Schematic illustration of magnetic surface molecularly imprinted polymers (SMIP)/magnetic carbon nanospheres (MCNSs) synthesis, B) Field emission scanning electron microscopy (FESEM) image obtained for SNIP/MCNSs, and C) Adsorbed concentrations at the equilibrium by SMIP/MCNSs showing adsorption selectivity for quinolone over phenol and pyridine. Reproduced with permission.[193] Copyright 2020, Elsevier.

Magnetic carbon nanotubes (CNTs) are cost-effective and environmentally benign materials with remarkable adsorbent properties, whose functionalization allows for increased capacity and selectivity. Nanocomposite beads (Gel-CNT-MNPs; M_S: 31 emu g^{-1}) were produced by entrapping carboxylic acid functionalized multi-walled carbon nanotube (MWCNT) in gelatin A (Gel) and embedding iron oxide magnetic NPs (MNPs).[207] Gel-CNT-MNPs showed very high adsorption capacity for anionic direct red 80 (1428 mg g^{-1}) and cationic MB (714 mg g^{-1}), respectively associated to the positive surface charge of the gel together with complexation with embedded MNPs and to electrostatic interaction of MB with carboxyl groups on the functionalized CNTs surface.[207] Thiol functionalized magnetic CNTs (CNTs-SH@Fe_3O_4; SSA: 200 m^2 g^{-1}, M_S: 31 emu g^{-1}) displayed an adsorption capacity of 172 mg g^{-1} for Hg^{2+} (pH: 3–11, T: 298 K), selectivity (adsorption > 81% for Hg^{2+} while < 29% for Cu^{2+}, Mg^{2+}, and Zn^{2+}), and slight efficiency decrease (from 94% to 80%) after five cycles.[208] Oxidized MWCNTs decorated with silica coated copper ferrite ($CuFe_2O_4$/oMWCNTs; SSA: 182 m^2 g^{-1}, M_S: 0.004 emu g^{-1}) were produced by co-precipitation and hydrothermal reactions and displayed an adsorption capacity

© 2021 Wiley-VCH GmbH

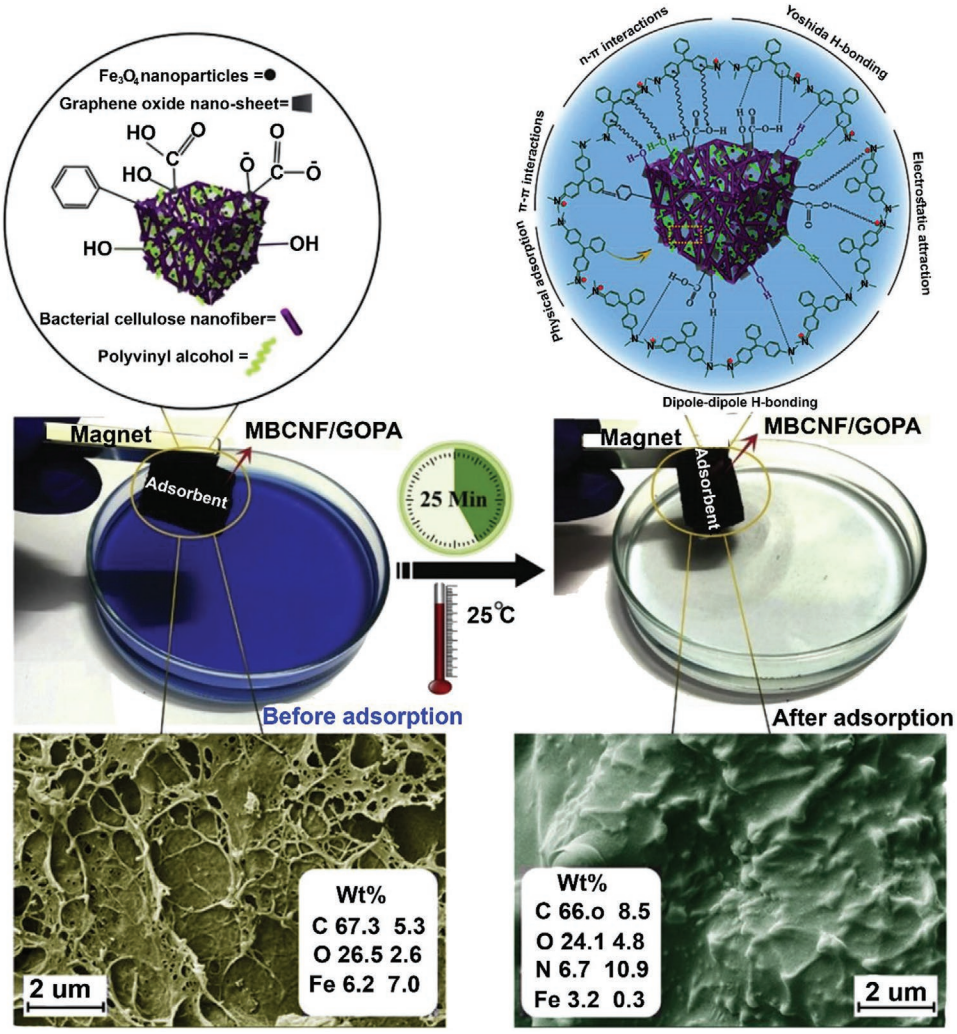

Figure 5. Representation of magnetic bacterial cellulose nanofiber/graphene oxide polymer aerogel (MBCNF/GOPA) before and after the adsorption of malachite green (MG) along with magnetic separation. For each case, the corresponding FESEM images and energy-dispersive X-ray spectroscopy (EDX) elemental composition are represented. Reproduced with permission.[198] Copyright 2020, Elsevier.

towards MB and celestine blue of 204 mg g^{-1} (pH: 5.6, *T*: 323 K) and 714 mg g^{-1} (pH: 5.5, *T*: 293 K), respectively.[209]

Magnetic Zeolites: Zeolites are porous crystalline aluminosilicates (natural or synthetic) with TO_4 tetrahedral units (T = Si, Al). These materials have many applications in the adsorptive treatment of water. Recently, zeolite-based magnetic composites have been developed. A smart Fe_3O_4@ZIF-90-cysteine was produced for the removal of Hg^{2+} by Nosike et al.[210] Fe_3O_4 NPs were capped with polyacrylic acid (PAA) to avoid their agglomeration, as described in **Figure 6**A. Then, the imidazolate framework ZIF-90, a promising zeolitic adsorbent, was used as core for the assembling of PAA-Fe_3O_4 NPs by a one-pot synthesis at room temperature. The resulting core-shell Fe_3O_4@ZIF-90, which was covalently bonded with cysteine in order to obtain Fe_3O_4@ZIF-90-Cysteine, is described in Figure 6B.[210] Because of the Fe_3O_4 core and cysteine bonding, the SSA decreased from ZIF-90 (1270 m^2 g^{-1}) to Fe_3O_4@ZIF-90 (222 m^2 g^{-1}) and Fe_3O_4@ZIF-90-Cysteine (96 m^2 g^{-1}, TEM image may be seen in Figure 6C). However, synergism between Fe_3O_4@ZIF-90-cysteine components allowed for high Hg^{2+} selectivity and adsorption capacity (900 mg g^{-1}) and good reusability (Figure 6E).[210]

Zeolitic imidazolate framework-8 (ZIF-8) was produced by the solvothermal method using cetyltrimethylammonium bromide (CTAB) and sodium dodecanoate as templates for adjusting the pore size. Then, magnetic ZIF-8@SiO_2@Fe_3O_4 (SSA: 1183 m^2 g^{-1}) aimed at ceftazidime removal was obtained from ZIF-8 and SiO_2@Fe_3O_4 self-assemblage, providing an adsorption capacity of 186 mg g^{-1} (pH: 6, *T*: 293 K) and maintaining efficiency (≥90%) after five cycles.[211] A faujasite zeolite was produced by a sol–gel process and decorated with $CoFe_2O_4$ NPs, resulting in a composite with high SSA (434 m^2 g^{-1}) and M_S (19 emu g^{-1}) that displayed 602 mg g^{-1} of Pb^{2+} adsorption capacity along with good reusability.[212]

Magnetic ZSM-5 zeolite was hydrothermally synthesized using tetraethyl orthosilicate as the silica source and sodium aluminate ($NaAlO_2$) as the aluminum source, which was then modified with NH_4Cl to produce magnetic H-ZSM-5 (SSA: 323 m^2 g^{-1}, M_S: 12 emu g^{-1}) with increased selectivity towards p-xylene (PX) and a 107 mg g^{-1} adsorption capacity

© 2021 Wiley-VCH GmbH

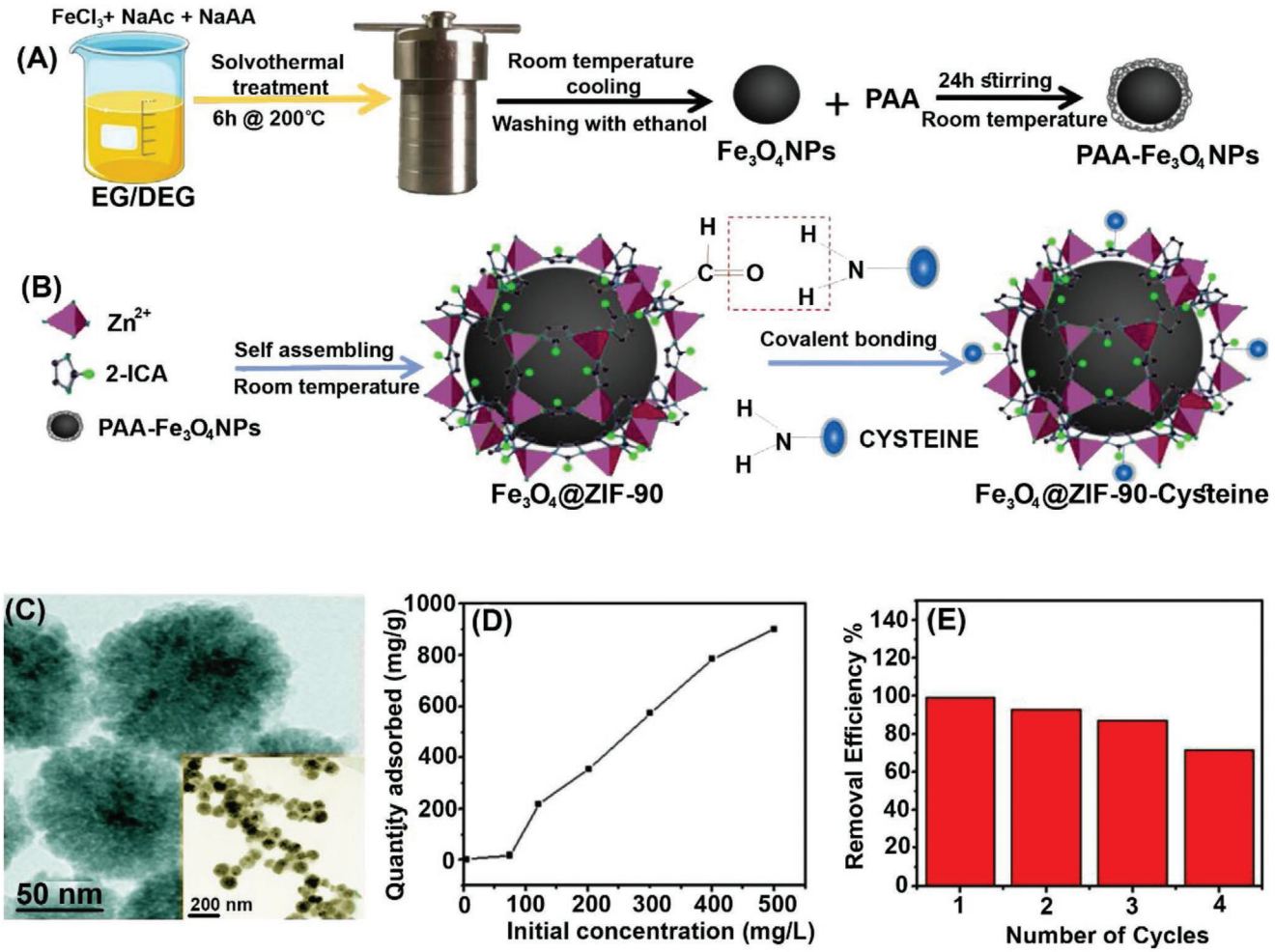

Figure 6. Synthesis routes for the production of A) Fe_3O_4 NPs capped with polyacrylic acid (PAA) (PAA-Fe_3O_4 NPs), B) Fe_3O_4@ZIF-90 and Fe_3O_4@ZIF-90-Cysteine, C) TEM picture of Fe_3O_4@ZIF-90 (inset of Fe_3O_4@ZIF-90-Cysteine), D) effect of initial Hg^{2+} concentration on its adsorption onto Fe_3O_4@ZIF-90-Cysteine, E) Hg^{2+} adsorption efficiency of Fe_3O_4@ZIF-90-Cysteine in subsequent cycles upon regeneration with 0.1 M HCl. Reproduced with permission.[210] Copyright 2020, Elsevier. Note: sodium acetate anhydrous (NaAc), sodium acrylate (NaAA), ethylene glycol (EG), diethylene glycol (DEG), polyacrylic acid (PAA), Imidazolate-2-carboxyaldehyde (2-ICA).

at 298 K.[213] Composites of Cu-exchanged zeolite A (Cu-ZEA; SSA: 16 m^2 g^{-1}), magnetite NPs, and either GO (Fe_3O_4/GO/Cu-ZEA; SSA: 29 m^2 g^{-1}) or reduced GO (Fe_3O_4/RGO/Cu-ZEA; SSA: 62 m^2 g^{-1}) were produced by solid-state dispersion with intercalated zeolite in graphenic layers resulting in increased *SSA* and arsenic removal.[214]

Magnetic Silica Based Adsorbents: MS possesses relevant adsorbent characteristics, namely large surface area, narrow pore size distribution, ordered structure, high thermal stability, and reliable desorption performance. To broaden its potential applications, endowing silica-based adsorbents with magnetic properties has being intensively explored during the last decade. Nanosized magnetite (NSM) was coated with MS shells to produce NSMSiO_2, which was used for humic acids and MG cationic dye adsorption, reaching capacities of 8 mg g^{-1} (≈5× more than bare SiO_2) and 542 mg g^{-1}, respectively.[215] A core–shell magnetic MS composite was subjected to functionalization with polyethylenimine to produce Fe_3O_4@SiO_2-PEI (SSA: 86 m^2 g^{-1}, M_S: 62 emu g^{-1}), which was characterized and used for silver NPs adsorption with a capacity of 909 mg g^{-1} (5–181× larger than previously published values).[216]

Hollow mesoporous silica spheres (HMSS) with SiO_2 sheets assembled as shells, were solvothermally produced.[217] Then, monodispersed Zn-doped Fe_3O_4 NPs were loaded on the SiO_2 sheets to obtain magnetic HMSS (MHMSS; SSA: 191 m^2 g^{-1}, M_S: 2.9 emu g^{-1}) for MB adsorption at a very fast rate (equilibrium attained in 1 min) and capacity.[217] The thiol-ene click reaction, which is advantageous over cross-linking methods, was used for synthesizing a magnetic mesoporous silica/chitosan (MMS/COS) composite with large Hg^{2+} adsorption capacity (438 mg g^{-1}), high selectivity, and good reusability (380 mg g^{-1} of capacity after six cycles).[218]

Imparting magnetic properties to different types of adsorbent materials is a hot research topic within the scientific community for the adsorptive treatment of water. A huge number of manuscripts have been published on magnet-responsive adsorbents during the last five years. This is an indication of the importance of after-use separation and the researchers'

© 2021 Wiley-VCH GmbH

desire to develop materials that may be implemented for water remediation in a sustainable way, with good regeneration and reutilization. Still, as shown in this section, most published results were obtained at a laboratory scale, with a special focus on adsorptive performance and with magnetic properties (mainly M_s) being used to support the possibility of after-use separation by a magnetic field. We believe that a myriad of smart magnet-responsive materials with remarkable properties have already been and are being developed. Thus, a step forward is needed towards application at pilot and real scale to fully prove their performance from the adsorptive, separation, regeneration, and reutilization points of view.

2.2. Multi-Stimuli Responsive Adsorbents

Multi-stimuli responsive smart materials are expected to eventually have the ability to replicate certain biological processes that can be utilized to clean the environment.[219] Hence, multi-stimuli responsive adsorbents intended for water purification, both at the bench scale and large scale application, can have biodegradation and biocompatibility capabilities.[220] The following section summarizes the performances of a variety of multi-stimuli adsorbent materials to highlight some of their interesting features.

The pH and temperature-responsive gellan gum-grafted-poly(2-dimethylamino) ethylmethyacrylate (GG-*g*-poly(DMAEMA)) hydrogel was synthesized through microwave-assisted free radical induced polymerization methodology for methyl orange (MO) adsorption from water.[221] The maximum MO uptake (C_o: 100 mg L^{-1}) of 25.8 mg g^{-1} (pH: 3), was attributed to interactions between the protonated tertiary amino group of DMAEMA polymeric chains and negatively charged sulfonate groups of MO molecules. Maximum adsorption was achieved at 30 °C, with a minimum at 50 °C (LCST of PDMAEMA) because the hydrogel becomes compact due to hydrophobic interactions between DMAEMA polymeric chains. Thus, poly(DMAEMA) imparts both pH and temperature-responsive characteristics to the polymeric hydrogel.[221]

A dual-responsive hydrogel based on GO was prepared by in situ radical copolymerization of the temperature-sensitive PNIPAM, and the pH-sensitive AA. The resulting hydrogel, GO/PNA, was tested for adsorption and desorption of Rhodamine B (RhB), and imidacloprid (IM).[222] The maximum adsorption of RB on GO/PNA was 193 mg g^{-1}, while 93% of the dye could be desorbed within 10 h at pH: 4.01 and *T*: 60 °C.[222] Swelling tests confirmed thermal and pH-responsive characteristics of the GO/PNA hydrogel. Morphologically, at pH: 4.01 and *T*: 25 °C, the GO/PNA hydrogel surface was coarse, while a smooth GO/PNA surface was observed at pH: 9.2. PNA carboxyl groups are protonated (−COOH) at low pH, while under neutral and alkaline conditions they are deprotonated ($-COO^-$), this results in swelling due to electrostatic repulsive forces among the groups. The relationship between water retention capacity and soaking time was also measured at temperatures above LCST (≈27 °C), and it was observed that the GO/PNA hydrogel shrunk when immersed in water heated from 40 to 70 °C. Moreover, the swelling ratio for the GO/PNA hydrogel was greater than 90% after five cycles.

A thermal and pH-responsive PNIPAM grafted COS/magnetite composite (COS-MCP), adsorbent was synthesized for the removal of nonylphenol (NNP) from water.[223] The pH-responsiveness was confirmed by the zeta potential-pH profile with a ≈9.5 isoelectric point. Under acidic conditions, the primary amino groups of pH-sensitive chitosan are positively charged, these ammonium ions then become unprotonated gradually as pH rises. Compared to CS-MCP (COS magnetic composite particles without PNIPAM), the zeta potential values of CN-MCP were nearer to zero, ascribed to the charge shielding effects of the non-ionic PNIPAM.

A contact angle study carried out at 20 and 40 °C proved the thermal-responsive nature of CN-MCP, with a water contact angle of 9.24° at 20 °C, that increased to 50.34° at 40 °C.[223] Thus, it could be inferred that the better adsorption performance of CN-MCP at 20 °C, was possibly due to the formation of a more hydrophilic form of NNP than at 40 °C. A slight decrease in CN-MCP particle size from 3.36 µm at 20 °C to 3.13 µm at 40 °C was due to collapsed branches, rather than extended branches of the hydrophobic PNIPAM as the temperature was above the LCST of PNIPAM (30 and 35 °C). Fractal dimension measurements showed a reduction from 2.47 to 2.44 with rise in temperature, indicating formation of more pores during the PNIPAM branching collapsing process.[223] At pH: 9 and *T*: 20 °C, the adsorption of NP was governed through electrostatic attraction and ion-exchange, while at pH: 5 and *T*: 40°C, hydrophilic interaction between NP and PNIPAM branches on CN-MCP played a key role during NP adsorption.

A pH and magnetic field responsive GO/poly(*N*-vinylimidazole-*co*-AA) hydrogel (MGO/PNA) was synthesized by random copolymerization of anionic AA and cationic *N*-vinylimidazole (NVI) in the presence of MGO in aqueous medium.[142] The adsorption of cationic and anionic dyes over MGO/PNA was also studied. It was found that highly acidic (pH ≈ 2) conditions favored anionic dyes adsorption due to electrostatic interactions between the sulfonic group of the anionic dyes and the protonated carboxyl group of the MGO/PNA hydrogel.[142] At high pH (≈12), cationic dyes adsorption was dominant due to electrostatic interaction between the deprotonated carboxyl group of the PAA segment and cationic dyes. Additionally, hydrogen bonding, van der Waals forces, π–π stacking and hydrophobic interactions further improved dyes adsorption on the MGO/PNA hydrogel. The superparamagnetic behavior along with an M_s value of 3.1 emu g^{-1} suggested ease in separation of the used adsorbent with an external magnetic field.[142] Desorption of cationic dyes was favored at pH: 2, while desorption of anionic dyes was favored at pH: 12.[142]

Thermal and magnetic dual-responsive NPs ($Fe@SiO_2$@PNIPAM) with an ultrafine $Fe@SiO_2$ inner core and PNIPAM shell were fabricated for the adsorption of phenolic compounds, including BPA, tetrabromobisphenol A (TBBPA), 4-*tert*-octylphenol (4-OP) and 4-*n*-nonylphenol (4-NNP) from water.[53] Temperature-dependent adsorption with a maximum uptake at 32 °C was observed, which is the LCST of PNIPAM. At temperatures below and above the LCST, hydrogen-bond interactions and hydrophobic interactions respectively played important roles in the adsorption of phenolic compounds. Thus, since relevant adsorption was also observed at 40 °C, it was inferred that the contribution of hydrophobic interactions during adsorption

© 2021 Wiley-VCH GmbH

was greater than hydrogen bond interactions. Adsorption capacity followed the trend 4-NP>4-OP>TBBPA>BPA.[53] The maximum amount of 4-NP (92.7%) was recovered using a methanol and ultrapure water (75:25%, v/v) mixture as eluent at 25 °C. The selected temperature for elution was most unfavorable for the adsorption of 4-NP as the PNIPAM layer was fully stretched at this temperature. The highest elution efficiency (92.74%) was achieved by the eluent with 75:25 methanol: water content.[53] The thermal-responsive adsorbent allowed for reduced organic solvent's usage as the eluent and after eight regeneration cycles, there was no significant decline in 4-NP adsorption. Furthermore, the saturation magnetization value of $Fe@SiO_2@PNIPAM$ was 24.855 emu g^{-1}, which was adequate for magnet-responsive separation.[53]

A mechanical and chemical-stimuli responsive cylindrical-drum-shaped Pd_2L_4-type coordination cage supramolecular gel was molded by complexation of $Pd(NO_3)_2$ with *N,N′*-bis(3-pyridylmethyl)-napthalenediimide (L) for selective removal of anionic dyes, viz. acid blue 93 (AB93) and MO in the presence or absence of cationic dyes.[224] Thixotropic (flows under shear force and solidifies on force removal) and reversible chemical-stimuli responsive behavior of 1.3% gel in dimethyl sulfoxide and MeCN-H_2O, acetonitrile-water (1:1) was found.[224] Therefore, phase transition from solid to gel and from gel to solid could be achieved by physico–chemical impacts. The porous gel network with cationic cage and napthalenediimide (NDI) core showed complete removal of AB93 and MO within an hour in a unary-system, while in a binary-system (containing AB93 and cationic RhB) only AB93 was selectively removed.[224] Electrostatic interactions with the metal center and NDI moieties were responsible for the binding of anionic dyes.[224]

A self-adhesive, self-healing, triple-stimuli (pH, temperature, and light) responsive hydrogel was synthesized by a hybrid system based on a tuneable composition of PDA and a polymer network composed of poly(*N,N*-diethylacrylamide-*co*-acrylic acid) (P(DEAA-AA)).[66] The resulting PDA@P(DEAA-AA) hydrogel displayed excellent self-adhesion (due to the abundance of free catechol groups) and self-healing (owed to the synergistic effect of PDA NPs and the polymer network) characteristics. *N, N*-diethylacrylamide (DEAA) and AA acted as temperature and pH-sensitive moieties and PDA NPs provided functional reinforcement. MB was tested as a model adsorbate, with a maximum adsorption of 388.8 mg g^{-1}, at pH 10, due to the presence of deprotonated carboxylic ($-COO^-$) groups. The PDA NPs in the hydrogel could convert the absorbed light energy into heat, consequently shrinking the temperature-sensitive component structure of the hydrogel's internal network, resulting in reduced MB uptake under stronger near-infrared illumination. Thus, the PDA acted as a molecular switch under the action of near-infrared light. The maximum adsorption of MB on PDA@P(DEAA-AA) hydrogel was 303.3 mg g^{-1} at 25 °C but decreased with increasing temperature. Above 25 °C, the interaction of hydrophobic groups in the DEAA moiety strengthened, forming a hydrophobic film, while destroying hydrogen bonds and solvation layers.[66] This resulted in the collapse of polymer chains present in the hydrogel, which caused shrinkage of the hydrogel volume, consequently decreasing MB adsorption on the PDA@P(DEAA-AA) hydrogel.[66]

A reversible pH, temperature, and mechanical stimuli-responsive supramolecular organo-gel (2-OA) was synthesized, through non-covalent interactions between tetrazolyl derivative and octadecylamine (OA).[225] 2-OA adsorbed dyes and heavy metals ions and had self-healing properties. Upon addition of acetic acid (HOAc), this organogel turned into a suspension as primary amine units of OA got protonated by acid addition. The opaque gel was subsequently restored by addition of diethyl amine (DEA) which led to the disassembly of the gel network.[225] The 2-OA gel transformed to suspension at temperatures > 60 °C and transformed to gel upon subsequent cooling to room temperature. Vigorous shaking transformed the 2-OA organogel into a suspension, which reverted to gel form when rested for two hours (a shearing-induced responsive behavior). This remarkable self-healing property is associated with the reforming of hydrogen bonds in the network of the 2-OA gel. In a unary-system, the maximum uptakes of bromophenol blue (BrB), MB, RhB, and MO dyes on 2-OA were 2607, 116, 1200, and 804 mg g^{-1}, respectively, while maximum uptakes of Cu^{2+} and Fe^{2+} ions on 2-OA were 1105 and 238 mg g^{-1}, respectively.[225] Binary studies showed 46% Cu^{2+} and 99.8% MO uptakes from their mixture, while the observed uptake from the Cu^{2+} and RhB mixture was 40% and 99.8%, respectively. Dye desorption from saturated 2-OA was possible by adding HOAc (this destroyed the gel network) and reversible adsorption was achieved upon addition of DEA. A few drops of methanol extracted the dye from the adsorbent which precipitated out in water. Thus, the 2-OA gel could be easily recycled upon solvent removal. **Table 3** summarizes some other stimuli-responsive smart adsorbents for water remediation and includes data on their adsorptive performance.

3. Selectivity of Adsorbents

Functionalization can bring about significant morphological and chemical improvements in an adsorbent. Morphological enhancements include larger surfaces, more abundant functional sites 'ready' for housing interactions, and more favorable porosity distributions. Grafting of functional groups such as hydroxyl, carboxyl or amide groups onto the virgin material are examples of chemical improvements.

Functionalization of the parent materials can induce selectivity in the resulting material.[231–234] A chelating adsorbent material (namely, 2-imino-4-thiobiuret attached to partially reduced GO) was prepared by amidinothiourea functionalization of GO. This improved adsorption selectivity for Hg^{2+} uptake at an adsorption capacity of 624 mg g^{-1} and 100% removal for [Hg^{2+}] up to 100 ppm. This adsorbent is one of the best carbon-based materials having a high Hg^{2+} (aq.) removal capacity.[234] The removal of Hg^{2+} by the 2-imino-4-thiobiuret–partially reduced GO in a mixture comprised of Zn^{2+}, Ni^{2+}, Cd^{2+}, Cu^{2+}, and Pb^{2+} (each 10 ppm) resulted in: <10% removal for each of Zn^{2+}, Ni^{2+}, and Cd^{2+}, 21% for Cu^{2+}, 63% for Pb^{2+}, but 100% for Hg^{2+}.[234] Recently, a coumarin derivative-anchored to an aminated halloysite nanotube-based chemosensor (CHNTs) was fabricated through the condensation of aldehydes and amides. These CHNTs were endowed with a "turn-on" fluorescence response resulting in a prominent fluorescence enhancement

© 2021 Wiley-VCH GmbH

Table 3. Summary of multi-stimuli responsive SMART adsorbents for water remediation.

Adsorbent	Stimulus/ stimuli-response	Synthesis method	Adsorption capacity	Remark	Ref.
Fe_3O_4/PMA-*g*-PVA	pH/magnetic	Topological transformation	Ag^+: 93.2 mg g^{-1}; Ni^{2+}: 48.0 mg g^{-1}; Cd^{2+}: 94.7 mg g^{-1}; Pb^{2+}: 139.2 mg g^{-1}; Co^{2+}: 45.27 mg g^{-1}.	Drastic increase in adsorption with increase in pH from 4 to 7 due to electrostatic forces and morphological changes. Rapid adsorbent separation under external magnetic field.	[44]
Fe/Cu-GO nanocomposite	pH/magnetic	Ex situ synthesis and electrostatic interactions	Tetracycline: 201.9 mg g^{-1}	97% tetracycline removal at pH < 8 within 15 min. Nearly 100% tetracycline after five consecutive regeneration cycles at pH > 8.	[226]
P(NIPAM-AM-MA) hydrogel	pH/temperature	Free radical polymerization	Cu^{2+}: 25 mg g^{-1} at pH: 5, 30 °C	Higher adsorption of Cu(II) occurred below LCST. The Cu(II) loaded hydrogel was easily regenerated by 0.1 M HCl, which allowed for recovering more than 90% Cu(II) in 30 min. High regeneration efficiency after three desorption cycles.	[227]
PMOA/AT-Fe_3O_4 hydrogel	pH/temperature/ magnetic-field	In situ free radical polymerization	RhB: 2.11 mg g^{-1} at 25 °C	Significant RhB uptake was observed near LCST under acidic pH conditions. The application of an external magnetic-field not only allowed for the adsorbent separation but also improved the dye uptake capabilities of the hydrogel.	[228]
P-(NIPAM-MA-VI)	pH/temperature/ metal ion	Free radical polymerization	Cu^{2+}: 21.1 mg g^{-1} at pH: 5 and 60 °C	Temperature and pH induced four distinct phase transitions above critical concentration. Carboxylate (chelation due to electrostatic forces) and deprotonated imidazole (coordinate bond formation) ions governed Cu(II) adsorption.	[229]
Azine-containing bispillar[5]arene-based supramolecular pseudopolyrotaxane gel	Temperature/ acid and base concentration/ competitive guest	Host-guest interactions, π–π stacking interactions and hydrogen bonding interactions	RhB: 97.6%	Reversible sol-gel transitions were observed with changes in temperature and concentration, while acid, base, and the presence of competitive guest resulted in irreversible transitions.	[230]

at 444 nm when exposed to Zn^{2+} ions.[235] It was inferred that the "turn-on" fluorescence feature of the CHNTs helped to induce the yield high adsorption capacity and high selectivity for Zn^{2+} ions over other competing metal ions because of intermolecular π–π interactions.[235]

A novel poly (1,4-diazocane-5,8-dione) macrocyclic-functionalized hydrogel adsorbed iron with greater capacity than in Fe/Cr, Fe/Cu, Cu/Cr, Fe/Cu/Cr, and Fe/Cr/Cu/Co/Ni competitive ion systems.[236] Recently, a water-stable MOF/polymer composite, Fe-BTC/PDA (where Fe/BTC is the MOF and BTC is 1,3,5-benzenetricaboxylate) (**Figure 7**A,B), was capable of fast and selective uptake of large amounts of Pb^{2+} and Hg^{2+} from real world water samples.[237] This composite (Figure 7A) has a large cage morphology within the Fe-BTC structure with PDA embedded within the porous channels.[237] This composite had a very rapid uptake (within seconds) of up to 1634 mg g^{-1} of Hg^{2+} and 394 mg g^{-1} of Pb^{2+} with a removal efficiency >99.8% from 1 ppm-solution.[237] In contrast to Fe-BTC, the Fe-BTC/PDA composite considerably enhanced the removal of all metals except Cr^{6+}.[237] Additionally, it decreased the Pb^{2+} concentration down to safe drinkable levels (Figure 7C).[237] Hence, the Fe-BTC/PDA composite turned out to be a unique material having remarkable selectivity for Pb^{2+} removal from real world water samples (Figure 7D).[237] 1,2,4,5-benzenetetracarboxylic acid-functionalized magnetic NPs (Fe_3O_4@BTCA) were synthesized as shown in **Figure 8** when they were applied as an adsorbent for Congo red (CRd) (Figure 8A–D). Fe_3O_4@BTCA selectively adsorbed CRd dye at a capacity of 630 mg g^{-1} (Figure 8E). Attraction to the adsorbent was due to strong H-bonding between BTCA and CRd dye.[238]

More novel materials having unique properties and remarkable adsorption capabilities under specific reaction conditions are being designed and synthesized. The corresponding assessment of adsorbent selectivity is gaining popularity and significance. The determination of 'selectivity' for a specific species has been calculated using different metrics. Selectivity has been assessed, for example, as the binding selectivity coefficient which is inversely linked to the competitive binding affinity of a specific target molecule competing with other molecule(s) at a common adsorbent binding site.[239] Selectivity has also been determined as a selectivity coefficient. This is defined as the ratio of distribution coefficients $K_{Pb^{2+}}$ to $K_{M^{2+}}$ (M being other competitive heavy metal ions).[240] Selectivity has also been discussed in the following forms: as a separation factor SF_X^Y defined as separation of X and Y and evaluated as the ratio of the distribution coefficient of X (K_d^X) to that of Y (K_d^Y).[241] Another definition is the selectivity separation factor defined as α_M^{Li} for the novel photo-responsive Li ion imprinted polymers for Li^+ (M is the other ion),[242] where a relative selectivity separation factor was defined as α_r and evaluated as the ratio of the selectivity separation factor of photo-responsive Li ion imprinted polymers for Li^+ to that of photo-responsive non-ion imprinted polymers.[242]An ideal adsorption selectivity index was also formulated having the format $S = (q_1/C_1)/(q_2/C_2)$

© 2021 Wiley-VCH GmbH

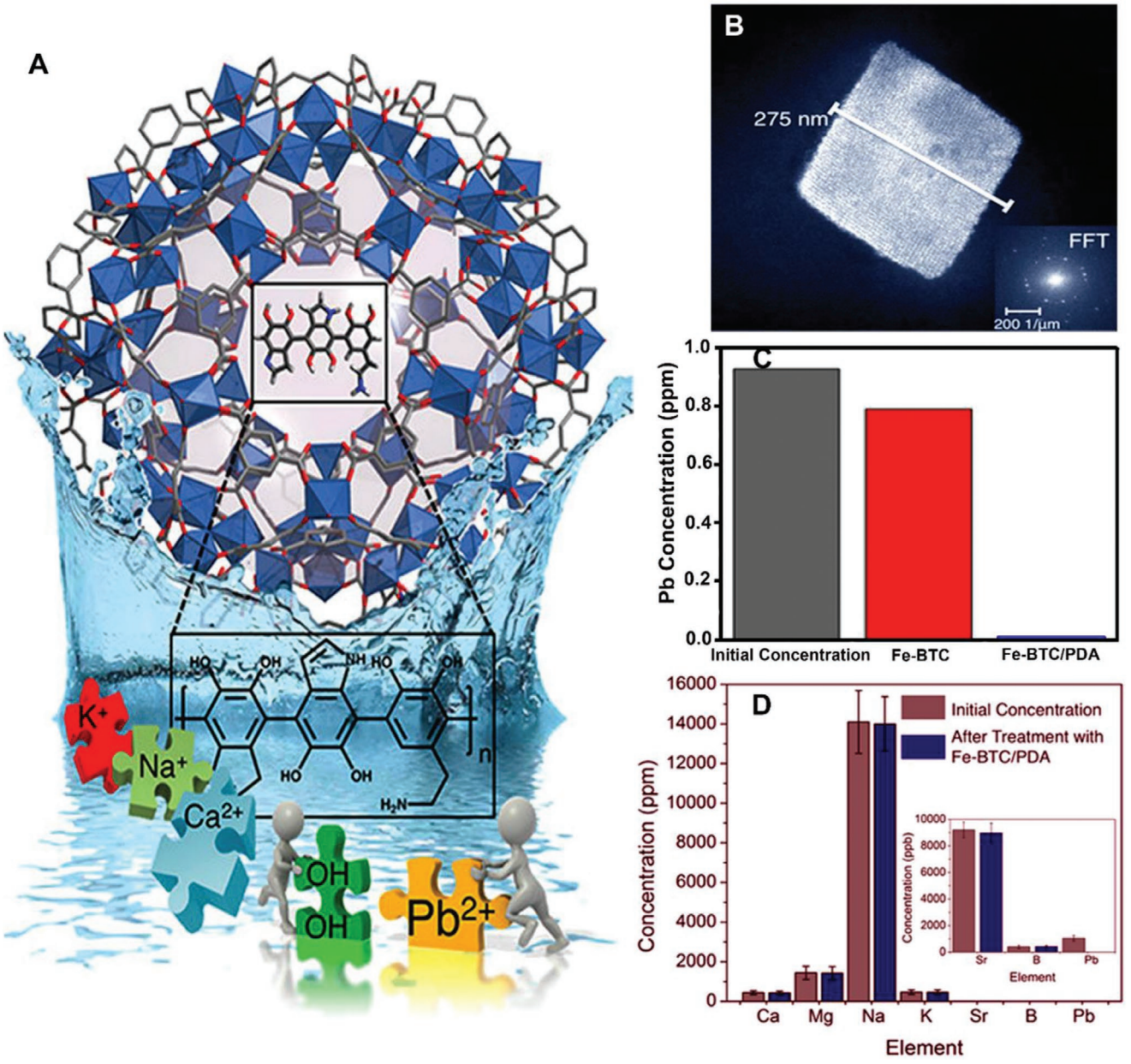

Figure 7. A) Graphical illustration of the metal–organic framework/polydopamine (Fe-BTC/PDA) composite and its selective adsorption in a mixture of various metal ions, B) High-angle annular dark-field scanning transmission electron microscopy (HAADF-STEM) image of a sliced single crystalline of Fe-BTC/PDA-19 composite, C) Evaluation of Pb^{2+} removal. Pb^{2+} concentration in distilled water before treatment (grey) and after treatment with Fe-BTC (red) or Fe-BTC/PDA-19 (blue), and D) Evaluation of the selectivity of this adsorbent by Mediterranean Sea water as a real sample. Mediterranean Sea water was spiked with Pb^{2+} ≈1 ppm and then treated with Fe-BTC/PDA-19. The ion concentrations before and after treatment are signified as rosewood and blue, respectively. Reproduced with the permission.[237] Copyright 2018, American Chemical Society.

where q is the equilibrium adsorption capacity at any given concentration C of two test environmental contaminant species (1 and 2) involved (1 = MO and 2 = MB).[243]Finally, a selectivity coefficient $S_{Au/M}$ was defined where the adsorption of Au^{3+} (aq.) by glutaraldehyde-crosslinked chitosan beads was investigated, among other experimental conditions in competitive aqueous media.[244] There are other recent parameters which have been used to assess the selectivity of adsorption of contaminants by smart adsorbent materials, and these are reported in **Table 4**

Smart adsorbents will achieve a complete and significant meaningfulness when used in real world applications. These novel materials should be developed to attain commercial viability in large-scale pollutant adsorption and separation applications. Multiple stimuli-responsive adsorbents, which are actuated by two or more triggers, are still scarce and deserve more research and development efforts in the future. Smart adsorbent materials operating by different mechanisms, which could work collaboratively with a combination

© 2021 Wiley-VCH GmbH

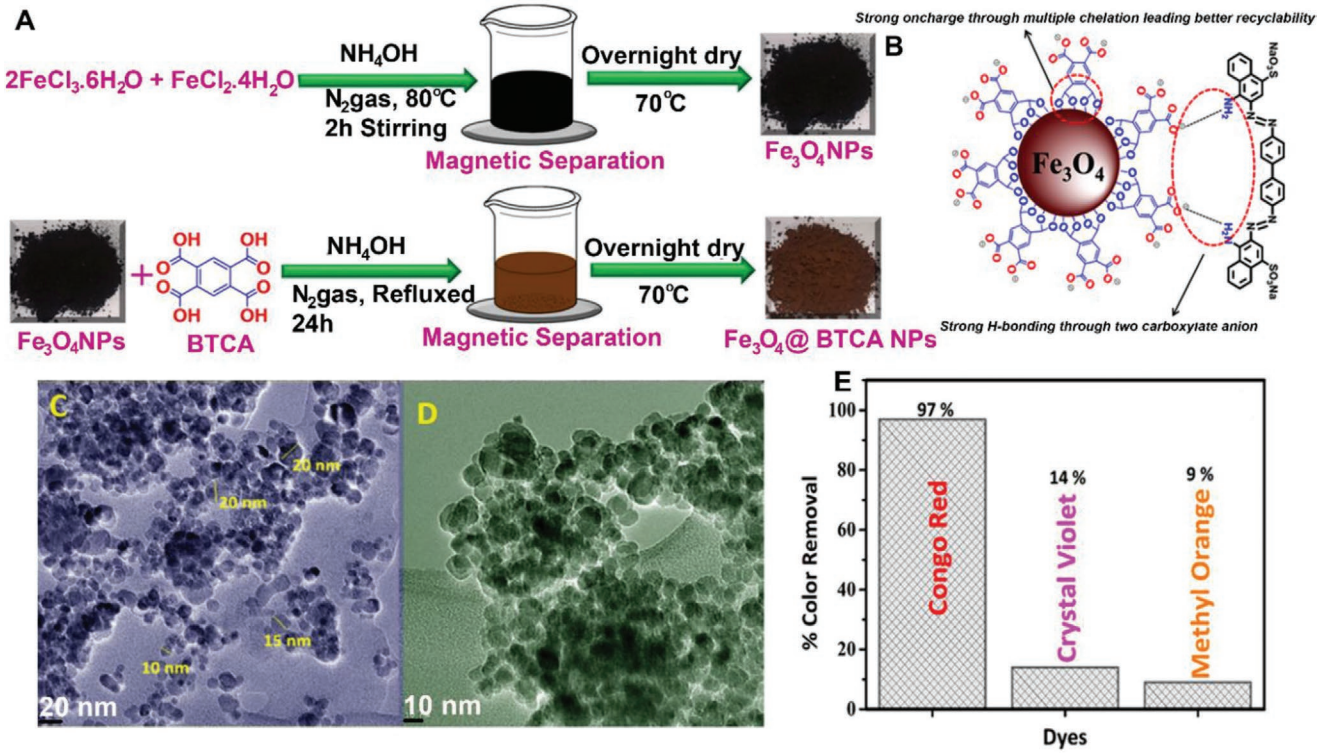

Figure 8. A) Graphical illustration of the fabrication of surface-modified magnetite 1,2,4,5-Benzenetetracarboxylic acid (Fe_3O_4@BTCA). The synthetic procedure included the Fe_3O_4 fabrication by co-precipitation of $FeCl_3$•$6H_2O$ and $FeCl_2$•$4H_2O$ in the alkaline condition and following immobilization of BTCA groups onto Fe_3O_4, B) Adsorption mechanism of congo red (CRd) dye occurred through H-bonding with carboxylate anions, C) Transmission electron microscopy (TEM) images of Fe_3O_4@BTCA, D) CRd dye adsorbed onto the Fe_3O_4@BTCA, and E) Bar diagram for percentage removal of CRd, crystal violet (CV), and methyl orange (MO) which showed selective adsorption of CRd. Reproduced with the permission.[238] Copyright 2020, Nature.

of different triggers, are expected to synergistically promote pollutant adsorption.

Real contaminated milieus are highly complex[4,248] and operate in 'harsh' environments consisting of many other chemicals.[246,249–252] Furthermore, they co-exist under variable temperatures, pH values and a variety of organic contents (such as humic acid,[253] protein-like organic matter[254] or lipids and nucleic acids[255]). These complications are enhanced by different ionic strengths, light intensity and flow rates. Limiting remediation performance to the sole adsorptive removal of a single target chemical is not plausible in real world scenarios. This is because coexisting contaminants will lower selectivity of the smart adsorbent for the targeted species. For example, based on risk quotient (RQ) evaluations, a high ecotoxicological risk was inferred due to erythromycin, clarithromycin, ofloxacin, sulfamethoxazole, and fluoxetine detected in the influent and effluent of a municipal wastewater treatment plant.[256] Conventional treatment methods were inadequate in effectively removing these micropollutants.[256] In another study, RQ values of more than unity for thirty compounds in secondary treated wastewater were reported (for example, RQ = 2.4 for Atorvastatin in *Daphnia magna*, RQ = 15 for Azithromycin in algae, RQ = 38 for Pentobarbital in algae, RQ = 927 for Caffeine in algae, RQ = 31 for Clarithromycin in algae, RQ = 835 for Nonylphenol in fish, RQ = 67 for Nonylphenol in *D. magna*, RQ = 30 for Nonylphenol in algae, RQ = 4914 for Triclosan in algae, and RQ = 13 for Tramadol in *D. magna*).[257] This mixture of micro-contaminants could induce significant ecological risk, even in rivers having dilution factors of 2388.[257] Algae were found vulnerable to Triclosan exposure in the aquatic environment but Triclosan did not induce any significant risk to human health.[258] Nevertheless additional wastewater treatment was recommended to completely remove triclosan residues.[258] It is hence important to determine and compare measured environmental concentration (MEC) and the predicted no-effect concentration (PNEC) for the environmental pollutants concerned,[256,259] because both are used in the evaluation of RQ (= MEC/PNEC).[256,257] Many reports consider the bioaccumulation of heavy metals (e.g. refs. [260–263]) and organic pollutants (e.g. refs. [264–266]) in living organisms, and some highlight potential impacts (such as toxicity) of heavy metals[262,267–272] and organic pollutants[16,264,273] even at low concentrations.

The merit of being classified as a 'selective' adsorbent should be cautiously articulated. Such designation must consider the relevant extent of legally and environmentally acceptable decontamination for each component[274] in real world remediation applications. Specific guidelines are often inadequate with regards to pollutant concentration control at different stages of effluent/contaminated water remediation.[275,276] This can then render the widespread usage and assessment of performance of a specific smart adsorbent challenging to compare and optimize. Ideally, the smart adsorbent(s) material should be potent enough to take up the target pollutants from a common competitive milieu with high adsorption capacity. Hence, the versatility

© 2021 Wiley-VCH GmbH

Table 4. Selective adsorption of contaminant species onto smart adsorbent materials.

Adsorbent material	Contaminant	Selectivity aspect(s) in adsorption performance	Selectivity metric	Key interactions	Ref.
Molecularly imprinted polybenzimidazole (PBI) nanofibers	Oxidized organosulfur compounds	Selectivity for the target compounds with average adsorption capacities of 28.5 mg g^{-1} for benzothiophene sulfone, 29.8 mg g^{-1} for dibenzothiophene sulfone and 20.1 mg g^{-1} for 4,6-dimethyldibenzothiophene sulfone	Binding selectivity coefficient of 40.2 for benzothiophene sulfone-imprinted nanofibers, 12.9 for dibenzothiophene sulfone-imprinted nanofibers, and 10.9 for dimethyldibenzothiophene sulfone-imprinted nanofibers	Hydrogen bonding between sulfone oxygen groups with NH groups of the PBI π–π interactions between the aromatic sulfone compounds and benzimidazole rings	[239]
Ordered spatial chelate resins	Pb^{2+}	Excellent adsorption capacity for Pb^{2+} (387 mg g^{-1}) One resin named '*L*-POMe6' demonstrated excellent selectivity for Pb^{2+} removal in competitive heavy metal ions milieu comprising Hg^{2+}, Cu^{2+}, Co^{2+}, Zn^{2+} and Cd^{2+}	Relative selectivity coefficient of L-POMe6 for Zn^{2+}, Cu^{2+}, Co^{2+}, Cd^{2+} and Hg^{2+} were nearly 94.6, 31.5, 56.8, 23.6 and 5.6, respectively	L-POMe6, behaving as a polydentate ligand, bonded with the metal ions	[240]
Organic-inorganic hybrid material of phytic acid-modified titanate nanotubes	Uranium (VI)	Maximum sorption capacity of 1.16 mmol g^{-1} (under reaction conditions pH 5.0 and at 293 K)	Phytic acid-modified titanate nanotubes composite gave much higher sorption selectivity for U(VI) in comparison with Sr^{2+}, Cs^{+}, Ni^{2+}, Co^{2+} and Eu^{3+} as the interfering ions	Strong selectivity of phytic acid-modified titanate nanotubes towards U(VI) occurred as a result of inner-sphere complexation between surface-coated phosphate groups and U(VI)	[245]
Multi-template molecularly imprinted polymer (MIP)	Naproxen, diclofenac and ibuprofen	Selectivity order: naproxen < ibuprofen < diclofenac Multi template molecularly imprinted polymer showed high selectivity to naproxen, diclofenac and ibuprofen in the presence of fenoprofen and gemfibrozil	Imprinting factors (α_{imp}): naproxen 1.2, ibuprofen 1.4 and diclofenac 2.0 $\alpha_{imp} = \frac{K_D(MIP)}{K_D(NIP)}$ and Partition coefficient, $K_D = \frac{C_P}{C_S}$ C_S and C_P are the concentration of target compounds (mg L^{-1}) in solution and in polymer, respectively, at adsorption equilibrium. NIP stands for 'Non imprinted polymer'.	Chemisorption of naproxen, diclofenac and ibuprofen on homogeneous binding sites	[246]
Molecule and ion dual-imprinted polymer	λ-cyhalothrin (a pyrethroid pesticide) and Cu^{2+}(aq)	Rapid binding kinetics with maximum Langmuir-based monolayer adsorption of 120.8 µmol g^{-1} for λ-cyhalothrin and 101.7 µmol g^{-1} for Cu^{2+} (at 35°C) λ-Cyhalothrin and Cu^{2+} both have greater imprinting factor than the other structural analogues	Selectivity coefficient of diethyl phthalate, fenvalerate, Cd^{2+}, Fe^{2+}, and Ni^{2+} were 2.1, 1.9, 2.0, 2.3, and 2.213, respectively. Very high selectivity coefficient in multi-solute milieu thus indicated preferential affinity to templates (λ-cyhalothrin and Cu^{2+}) because of a good imprinting effect	Chemical chelating reaction principally determines of the Cu^{2+} rebinding onto molecule and ion dual-imprinted polymer through interaction between Cu^{2+} and nitrogen atoms of pyridine ring Hydrogen bonding as the major interaction explaining capture of λ-cyhalothrin molecules	[247]
Hydrogel prepared following a Schiff's base reaction	Micropollutants: methyl orange (MO), methylene blue (MB), fluorescein sodium, bisphenol A, 1-naphthyl amine, 2,4-dichlorophenol and toluene	A hydrogel named '**P5P5G**' had been synthesized using hydrazide-functionalized pillar[5]arene **P5-1** and 4-aldehydephenyl-functionalized pillar[5]arene **P5-2** Porous structure not only provided excellent adsorption ability to P5P5G hydrogel, but equally endowed it with selectivity during the adsorption process of the micropollutants because larger pollutant molecules could not easily enter into binding sites	Maximum amount of micropollutant adsorbed at equilibrium ($q_{max,e}$): MO 47.1 mg g^{-1}, MB 163.9 mg g^{-1}, fluorescein sodium 25.0 mg g^{-1}, bisphenol A 238.1 mg g^{-1}, 1-naphthyl amine 125.0 mg g^{-1}, 2,4-dichlorophenol 62.5 mg g^{-1}, and toluene 41.8 mg g^{-1}	Host–guest interactions between the pillar[5]arene macrocycle and micropollutant molecules	[248]

© 2021 Wiley-VCH GmbH

of a smart adsorbent could allow for multiple-pollutant control of real contaminated aqueous media.

4. Reusability, Self-Healing and Self-Cleaning Considerations

The "effective reusability" of an adsorbent implies its potential to be regenerated and reused for many cycles with a minimal decrease in performance.[277] Adsorbent reusability can be influenced by the adsorbent surface charge.[277] An increase of eluent concentrations improves desorption efficiency, but at high eluent concentrations, the adsorbent's structure can be affected and desorption efficiency can decline.[278] At high temperature, the adsorbate to adsorbent binding breaks more readily, increasing the release rate of adsorbates and enhancing desorption.[278]

The laboratory scale reusability of smart adsorbents has been particularly high with the number of recycles reaching fifteen (**Table 5**). However, recycling can lead to a decrease in the adsorption capacity of the adsorbent due to incomplete desorption, loss of active binding sites, surface precipitation and alterations in the adsorbent's porosity, pore sizes and *SSA*.[277,279,280] Recently, an important observation was made that there is an ignorance of the lifecycle of adsorbents.[281] Hence, expanding the assessment of the actual reusability and regeneration dynamics of smart adsorbent materials is required both at the research level and in large scale water treatment systems. The detailed adsorbent behavior within the different unit operations they are exposed to should be elucidated, and the results used to formulate a roadmap for their lifecycle. The recovery performance and reusability data for large scale application of smart adsorbents from lifecycle analysis are needed to determine the process-related operational[279,282,283] and maintenance costs,[284,285] and also in decreasing the generation of solid residues (e.g. sludge[286]). The most technically and economically appropriate desorption and adsorbent regeneration approach[287,288] (chemical and/or physical,[282] or biological[286]) for specific large scale smart adsorbent(s)-water remediation systems should be pre-examined and selected. Appropriate smart adsorbent selection should yield cost-effective recovery and regeneration rates downstream.

A combination of regeneration techniques can be effective in spent adsorbent recovery.[286] This can elucidate regeneration mechanisms involved and support overall regeneration optimization. Often multiple mechanisms impact regeneration dynamics of smart adsorbents which vary with varying physicochemical and biological conditions. Some smart adsorbent regeneration mechanisms involve the exposure of active sites which assists desorption. An example of this is the 4-(3-triethoxysilylpropyl-ureido)azobenzene molecular switches, which were photochemically converted to the trans configuration.[36] Another example is the temperature-induced re-swelling behavior observed with CF/poly(NIPAM-*co*-AAc).[109] Photo-responsive characteristics enabled the sorbate recognition sites of a photo-responsive cellulose-based intelligent imprinted material to preserve adequate consistency and significant recyclability.[38] Other examples include the pH-induced superwettability transition of a pH-responsive sponge,[289] and the Fickian diffusion-governed release of MB from a thiol-modified carboxymethyl cellulose nanocrystal hydrogel, named Cellulose-SH.[290] Finally, the dual effects of both switching solution pH and magnetic attraction of Fe_3O_4/PMA-*g*-PVA nanocomposites were evaluated to see how adsorption performance varied for Ag^+, Ni^{2+}, Pb^{2+}, Cd^{2+}, and Co^{2+} ion uptake.[44]

Two other important criteria related to regeneration and reusability of adsorbents are their self-healing[66,67,302–307] and self-cleaning[63,65,308–310] features. For example, the flexibility of carbon fiber was merged with the very high adsorptive capability of copper iodide (CuI) by preparing a CuI-homogeneous coating on carbon cloth (CuI@CC) adsorbent.[63] The CuI coating of this adsorbent imparts a self-cleaning property which enables the photocatalytic decomposition of adsorbed organics. This self-cleaning property permits the CuI@CC adsorbent to maintain its adsorption capacility through many reuse/regeneration cycles.[63] Pristine chitosan–grafted–polyN-Methylaniline (Ch-*g*-PNMANI) and the Ch-*g*-PNMANI-impregnated TiO_2 nanocomposites (Ch-*g*-PNMANI/TiO_2) had high adsorption capacities for remazol red RB-133 dye (116.3 mg g^{-1} for Ch-*g*-PNMANI/TiO_2 and 108.7 mg g^{-1} for Ch-*g*-PNMANI).[311] Both these adsorbents had good sunlight-assisted photoactive self-cleaning properties (photoactive adsorbents could still take up dye molecules after five adsorption/sunlight self-cleaning photoregeneration cycles with removal efficiency above 74%).[311]

Self-healable[66,70,302] and self-cleaning[63,64,312] adsorbents are gradually gathering research focus and interest. Adsorbents become more desirable when they are robust, cost-effective, and designed for large scale applications. Smart adsorbents, which may have unfavorable responses to one or more stimulus, can be damaged due to stress-governed crack formation.[70] This can affect material morphology and lower adsorption capacity and adsorption performance. Therefore, a research priority exists to develop smart adsorbents which can self-heal themselves by restoring their original morphologies and high-performance adsorption capacities. Exciting synthetic research efforts report several hydrogels and other novel materials such as self-assembled supramolecular gels,[225] metallogels,[306] and hyper-crosslinked metal–organic polyhedra.[307] These materials possess one or more of the following attributes: high stability,[225] outstanding mechanical properties,[313] and the ability to self-heal from chemical and physical damage,[306,314,315] and/or repeated damage.[316] For example, PDA composited LAPONITE crosslinked hydrophobically-associated hydrogels (PLHAhyds) have been synthesized by a facile in situ polymerization method.[67] Based on SEM results, it was observed that addition of LAPONITE content led to the PLHA gels developing a significantly denser and uniform morphology with a well-defined porous structure.[67] Interestingly, the incorporation of the LAPONITE nanosheets caused the wall thickness of the PLHA gels to be significantly increased in comparison with that of HA gel.[67] The PLHAhyd had enhanced mechanical features and LAPONITE endowed the novel material with very high stability through additional cross-linking.[67] The authors indicated that PDA, having an abundance of functional groups, can bind organic dyes and also ameliorate the self-healing characteristics of the hydrogel. The LAPONITE nanosheets also serve as second crosslinking points, thereby inducing an improvement

© 2021 Wiley-VCH GmbH

Table 5. Summary of the reusability performance of selected smart adsorbents used for sequestering inorganic and organic environmental pollutant species.

Adsorbent	Species adsorbed	Number of adsorption/ desorption cycles	Highlights of reuse potential	Ref.
Cross-linked pH-responsive tetrapolymer	Cr^{3+}	5	Ease of reusability and stable efficiency	[291]
2D magnetic poly($C_3N_3S_3$)/rGO nanocomposite	Pb^{2+}, Hg^{2+}	15	Adsorption capacities for Pb^{2+} and Hg^{2+} ions were stable because of Fe_3O_4 encapsulation within rGO-poly($C_3N_3S_3$) structure	[45]
$La(OH)_3$-modified magnetic $CoFe_2O_4$ nanocomposites	Phosphate	6	Adsorption efficiency diminished slightly but was more than 80% after 6 cycles	[292]
pH responsive nanogel made up of silica, magnetite, and poly(4-vinylpyridine)	Cd^{2+}, Cu^{2+}, Ni^{2+}, and Pb^{2+}	10	Repeated use without any significant loss in original binding affinity (2.2% relative standard deviation for 10 replicates with same adsorbent)	[293]
pH sensitive potential semi-IPN hydrogels made up of Pectin/poly(acrylamide-co-acrylamidoglycolic acid) with a *N,N'*-methylene-bis-acrylamide cross-linker	Cu^{2+} and Ni^{2+}	At least 5	Regeneration and use thereafter of hydrogels would improve economics of practical application for Cu^{2+} and Ni^{2+} ion removal from wastewater and water	[294]
Photo-responsive cellulose based intelligent imprinted material	2,4-dichlorophenoxyacetic acid	8	Very high stability, reusability, long working life and green regeneration	[38]
Dual (temperature and pH)-responsive polyethersulfone-poly (dimethyl amino) ethyl methacrylate blend nanofibers	Cu^{2+}	5	Nanofibers still capable of adsorbing Cu^{2+} after five adsorption cycles, although there had been a decline in efficiency.	[295]
Dual thermoresponsive mesoporous imprinted polymer	Cd^{2+}	5	No significant decline in adsorption capacity for 5 recycles of adsorbent	[296]
pH-responsive resin composed of zwitterionic aminomethylphosphonate ligands and hydrophobic 6-(biphenyl-4-yloxy)hexyl pendants	Cr^{3+}, MO, RhB, eriochrome black T, MB, methyl red	3	Resin had outstanding efficiency for Cr^{3+} uptake from waters after three cycles with ±4% changes	[297]
Water-stable cationic porous coordination polymer	ClO_4^-	5	After 5 successive cycles, removal efficiency remained above 85% Integrity of framework was assessed, and morphology of all crystals was also unaltered (i.e. unimpaired) after five cycles	[298]
Fe@SiO_2@PNIPAM	4-tert-octylphenol, bisphenol A, 4-*n*-nonylphenol, tetrabromobisphenol A	8 for 4-*n*-nonylphenol	Adsorption quantity of 4-NP showed no obvious decrease for 8 adsorption–desorption cycles	[53]
pH-sensitive and magnetically separable Fe/Cu bimetallic NPs supported by GO	Tetracyclines	5	Nanocomposite had high stability (near 100% removal of tetracyclines) still after five cycles	[226]
Chitosan-based magnetic microspheres grafted with Poly(DMAEMA)	Reactive Blue 19, Acid Green 25	5	High recovery efficiencies were still obtained after five cycles	[299]
La-MOF-NH_2@Fe_3O_4	Selective adsorption of CRd in presence of Sunset Yellow, MO, Fluorescein, Safranin, RhB, MB	5	Dye removal efficiency for CRd was above 90% after five consecutive regeneration cycles	[300]
Superabsorbent polymer hydrogel made up of acrylamide and acrylic acid	Ni^{2+}, Cd^{2+}, Cu^{2+}, Co^{2+}	5	No significant change in removal performance of hydrogel over five consecutive cycles	[43]
Dendrimer–modified magnetic NPs grafted to photo-responsive molecularly imprinted polymers (dMNPs@PMIPs)	Azathioprine	10	No visual alterations were observed in performance of dMNPs@PMIPs during the ten cycles	[301]

in mechanical performance.[67] An ionogel was produced from the ester functionalized pyridinium based ionic liquid based surfactant, that is, 1-*n*-hexadecyloxycarbonyl methylpyridinium bromide in aqueous medium.[70] This ionogel was demonstrated to have developed remarkable moldable, load bearing, self-sustaining, and self-healing features.[70] In particular, the opaque ionogel could selectively remove MO from an aqueous medium (99% removal efficiency in 20 h), and be also used repeatedly for up to 15 cycles with no loss in efficacy.[70]

In comparison of a mussel-inspired GO–based hydrogel with a hydrogel with no GO, the material with GO (5 wt%) had a ten-times greater storage and loss moduli, and a 104% and 134% increase in compressive and tensile strengths, respectively.[317] This polyaspartamide/GO hydrogel exhibited fast and

© 2021 Wiley-VCH GmbH

autonomous self-healing characteristics and strong hydrogen bonding. Boron–catechol coordinative bonding between polyaspartamide side chains and the GO nanosized sheets were thought to improve mechanical strength and gelation behavior following pH stimulation of the hydrogel.[317]

A reusable and entirely physically cross-linked GO/hydrophobically associated polyacrylamide composite hydrogel (GHA gel) was readily synthesized by including small quantities of GO with hydrophobically associated polyacrylamide (HAPAM).[304] In comparison with the HAPAM gel alone, the GHA gels produced had significantly higher tensile strength (242 kPa. This was attributed to strong hydrogen bonding interactions between the polymer chains and GO sheets.[304] The reorganization of the network structure of HAPAM enabled rapid recovery from damage, and this yielded GHA gels endowed with desirable anti-fatigue and self-healing properties.[304] Other self-healing systems have been made. A thermo-, pH-, and shearing-induced responsive 2-octadecylamine (**2**-OA) supramolecular gel had very high adsorption capability for ten types of anionic and cationic dyes, and for Fe^{2+} and Cu^{2+} ions, and even in co-adsorption systems for dyes and binary combinations of dyes/metal ions.[225] The **2**-OA gel demonstrated substantial elastic response and fast self-healing capability under oscillatory stress at room temperature. The self-healing characteristic emanated from the re-forming of hydrogen bonds within the gel network.[225] However, under another set of tests, the **2**-OA gel could not sustain macroscopic self-healing ability and molding because of a lower viscoelasticity resulting from a paucity of water-assisted hydrogen bonding.[225]

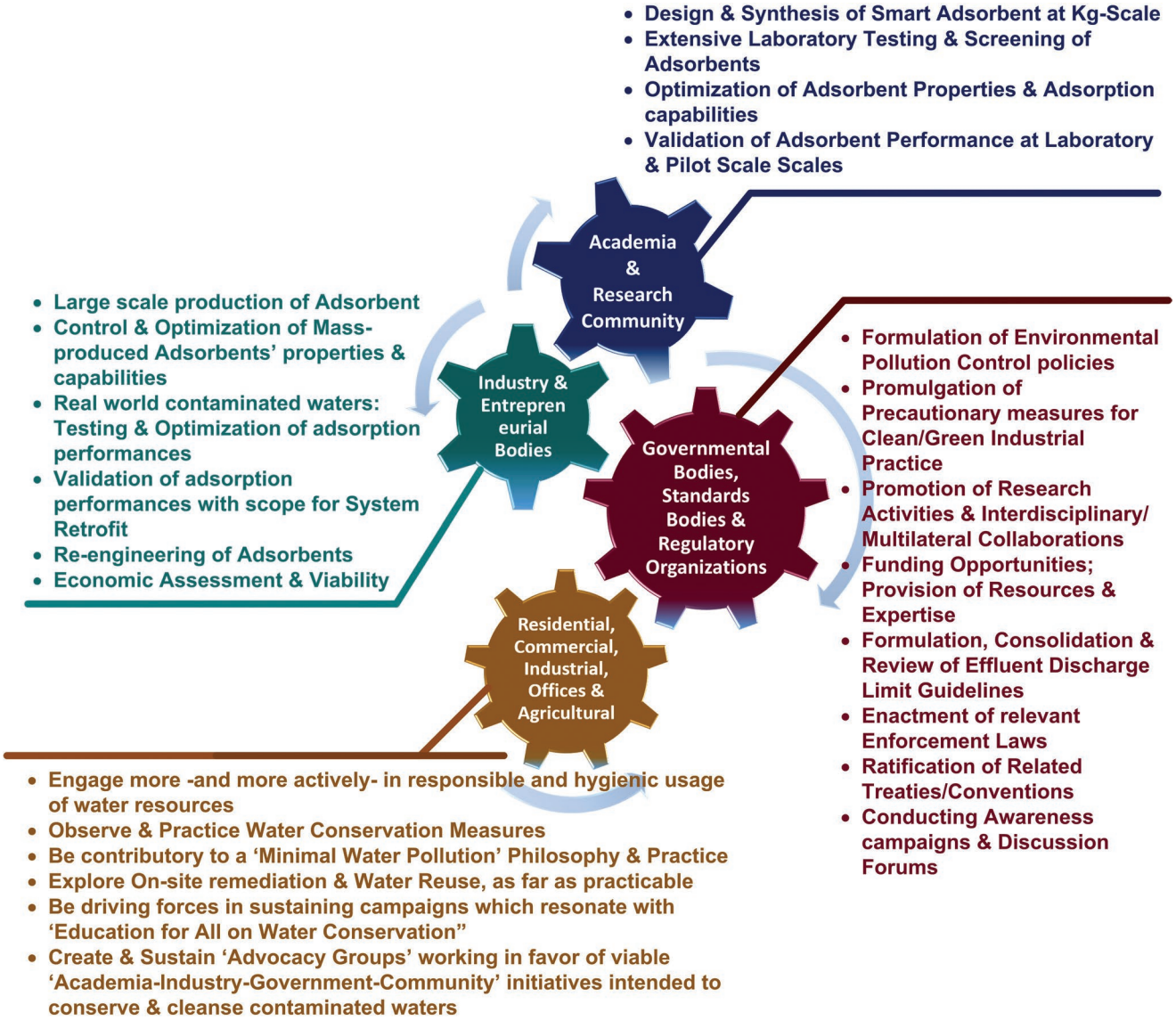

Figure 9. Summary of some core considerations for a consolidated way forward within the complex set of linkages connecting the academia, industry, government, community, and other related bodies around water treatment and water management issues.

© 2021 Wiley-VCH GmbH

5. Conclusion

Research in the synthesis and assessment of smart adsorbents has been quickly growing over the last decade. The smart adsorbent materials surveyed here have demonstrated very effective performances in taking up one or more chemical species from a single-adsorbate or multicomponent aqueous milieu under highly variable environmental conditions. Nevertheless, there are still many challenges to be addressed to widen the versatility of smart adsorbents for techno-economically viable application to real world systems. Multiple stimuli responsive adsorbent materials are still scarce. Hence, more research and development initiatives have to be geared to this area. Smart adsorbent materials having different adsorption mechanisms for the same or different environmental pollutants can be tuned to cooperate. More research and analysis are needed to elucidate the interrelationship(s) and mechanism(s) of interactions of stimulus-responsive smart materials under the influence of multiple stimuli operating concomitantly within the same environment.

Besides reaching the goals embodied in the acronym SMART, it is also imperative to perform reproducible and comprehensive toxicity and eco-safety analyses of the novel materials before they can be used for large scale treatment of water. The need to ensure the novel SMART materials are adequately safe and have a minimal disruptive set of impacts on the receiving ecosystems is motivated by the core premises of the parent concept of sustainability. Linked to sustainability, the use of eco-safe SMART adsorbents also requires that they are developed in a manner that is benign as possible. Throughout the entire lifecycle of the SMART adsorbents, it is crucial to explore and crosscheck ways to lower their ecological footprints. These ecological footprints broadly comprise inter alia, material use, energy consumption, synthetic reaction chemistries employed to produce the SMART adsorbents, and any biological, physical, and/or chemical conversions or degradation of the SMART adsorbents to unsafe products resulting in secondary pollution. They should also not cause metabolic disturbances in receiving biota. The literature contains some lab-scale toxicity assessment of novel adsorbents.[318–326] These data are derived for systems which do not mimic and capture the real lifecycle components and complexity of micro- and macro environments to which the SMART adsorbents can be exposed in real-world water treatment systems. They also do not account for how ecosystems downstream influence the final treated effluent discharge. Hence, besides ensuring an eco-design and eco-synthesis of SMART adsorbents, it will be imperative to assess their ecotoxicological behaviors and impacts in real (large-scale) water treatment environments. Such results can be useful in determining the improvements achieved, making waters more eco-safe and potentially suitable for real-world treatment applications.

Besides the core research developments, it will be crucial to establish new multiple-stakeholder partnerships (**Figure 9**) around the water treatment and management issues at the local, regional, national and international levels. Existing academia-industry-government-community linkages need to be deepened and strengthened to accelerate real world applications of all constructive advances covering smart adsorbents. Eventually they need to reach large scale water treatment systems.

Acknowledgements

E.N.Z. and A.M. contributed equally to this work. M.O. acknowledges FCT for the Investigator Program (IF/00314/2015) and FCT/MCTES for the financial support to CESAM (UIDP/50017/2020+UIDB/50017/2020), through national funds. The authors thank Professor Sanjay K. Sharma (Department of Chemistry, JECRC University, Jaipur, India) for sharing his thoughts on self-healing adsorbents. The TOC image contains icons created with BioRender.com.

Conflict of Interest

The authors declare no conflict of interest.

Keywords

metal ions, regeneration, smart adsorbents, selectivity, stimulus-responsive adsorbents, xenobiotics

Received: December 13, 2020
Revised: February 19, 2021
Published online:

[1] H. N. M. E. Mahmud, A. K. O. Huq, R. B. Yahya, *RSC Adv.* **2016**, *6*, 14778.
[2] Ihsanullah, A. Abbas, A. M. Al-Amer, T. Laoui, M. J. Al-Marri, M. S. Nasser, M. Khraisheh, M. A. Atieh, *Sep. Purif. Technol.* **2016**, *157*, 141.
[3] P. V. Nidheesh, M. Zhou, M. A. Oturan, *Chemosphere* **2018**, *197*, 210.
[4] P. Gago-Ferrero, A. A. Bletsou, D. E. Damalas, R. Aalizadeh, N. A. Alygizakis, H. P. Singer, J. Hollender, N. S. Thomaidis, *J. Hazard. Mater.* **2020**, *387*, 121712.
[5] M. de Oliveira, B. E. F. Frihling, J. Velasques, F. J. C. M. Filho, P. S. Cavalheri, L. Migliolo, *Sci. Total Environ.* **2020**, *705*, 135568.
[6] K. O. K'oreje, F. J. Kandie, L. Vergeynst, M. A. Abira, H. Van Langenhove, M. Okoth, K. Demeestere, *Sci. Total Environ.* **2018**, *637–638*, 336.
[7] F. M. Windsor, M. G. Pereira, C. R. Tyler, S. J. Ormerod, *Water Res.* **2019**, *163*, 114858.
[8] V. Lenters, N. Iszatt, J. Forns, E. Čechová, A. Kočan, J. Legler, P. Leonards, H. Stigum, M. Eggesbø, *Environ. Int.* **2019**, *125*, 33.
[9] C. Sophia A., E. C. Lima, *Ecotoxicol. Environ. Saf.* **2018**, *150*, 1.
[10] R. Fernández-Cisnal, M. A. García-Sevillano, T. García-Barrera, J. L. Gómez-Ariza, N. Abril, *Aquat. Toxicol.* **2018**, *205*, 76.
[11] A. Cachada, T. Rocha-Santos, A. C. Duarte, *Soil Pollution*, Elsevier, Amsterdam **2018**, pp. 1–28.
[12] C. A. Sandoval-Carrasco, D. Ahuatzi-Chacón, J. Galíndez-Mayer, N. Ruiz-Ordaz, C. Juárez-Ramírez, F. Martínez-Jerónimo, *Bioresour. Technol.* **2013**, *145*, 33.
[13] R. Valentino, V. D'Esposito, F. Ariemma, I. Cimmino, F. Beguinot, P. Formisano, *J. Endocrinol. Invest.* **2016**, *39*, 259.
[14] A. Sabarwal, K. Kumar, R. P. Singh, *Environ. Toxicol. Pharmacol.* **2018**, *63*, 103.
[15] G. Yang, C. Chen, Y. Wang, L. Cai, X. Kong, Y. Qian, Q. Wang, *Environ. Sci. Pollut. Res.* **2015**, *22*, 9307.
[16] R. Islam, S. Kumar, J. Karmoker, M. Kamruzzaman, M. A. Rahman, N. Biswas, T. K. A. Tran, M. M. Rahman, *Environ. Technol. Innov.* **2018**, *12*, 115.
[17] A. Rico, C. Sabater, M.-Á. Castillo, *Ecotoxicol. Environ. Saf.* **2016**, *127*, 222.

 © 2021 Wiley-VCH GmbH

[18] K. Pokorska-Niewiada, M. Rajkowska-Myśliwiec, M. Protasowicki, *Bull. Environ. Contam. Toxicol.* **2018**, *101*, 222.
[19] A. E. Burakov, E. V. Galunin, I. V. Burakova, A. E. Kucherova, S. Agarwal, A. G. Tkachev, V. K. Gupta, *Ecotoxicol. Environ. Saf.* **2018**, *148*, 702.
[20] S. Kim, K. H. Chu, Y. A. J. Al-Hamadani, C. M. Park, M. Jang, D.-H. Kim, M. Yu, J. Heo, Y. Yoon, *Chem. Eng. J.* **2018**, *335*, 896.
[21] E. Obotey Ezugbe, S. Rathilal, *Membranes (Basel)*. **2020**, *10*, 89.
[22] N. K. Soliman, A. F. Moustafa, *J. Mater. Res. Technol.* **2020**, *9*, 10235.
[23] C. Chen, Y. Kuang, L. Hu, *Joule* **2019**, *3*, 683.
[24] M. Ince, O. Kaplan İnce, *Int. J. Pure Appl. Sci.* **2017**, *3*, 10.
[25] H. Fu, X. Li, J. Wang, P. Lin, C. Chen, X. Zhang, I. H. (Mel) Suffet, *J. Environ. Sci.* **2017**, *56*, 145.
[26] F. Zietzschmann, C. Stützer, M. Jekel, *Water Res.* **2016**, *92*, 180.
[27] A. Bhatnagar, M. Sillanpää, A. Witek-Krowiak, *Chem. Eng. J.* **2015**, *270*, 244.
[28] J. Mo, Q. Yang, N. Zhang, W. Zhang, Y. Zheng, Z. Zhang, *J. Environ. Manage.* **2018**, *227*, 395.
[29] J. Dou, Q. Huang, H. Huang, D. Gan, J. Chen, F. Deng, Y. Wen, X. Zhu, X. Zhang, Y. Wei, *J. Colloid Interface Sci.* **2019**, *533*, 416.
[30] V. Arya, L. Philip, *Microporous Mesoporous Mater.* **2016**, *232*, 273.
[31] S. Babel, T. A. Kurniawan, *J. Hazard. Mater.* **2003**, *97*, 219.
[32] V. Krstić, T. Urošević, B. Pešovski, *Chem. Eng. Sci.* **2018**, *192*, 273.
[33] G. K. Sarma, S. S. Gupta, K. G. Bhattacharyya, *Environ. Sci. Pollut. Res.* **2019**, *26*, 6245.
[34] Y. Yu, L. Yu, K. Y. Koh, C. Wang, J. P. Chen, *Crit. Rev. Environ. Sci. Technol.* **2018**, *48*, 1127.
[35] S. Gu, X. Kang, L. Wang, E. Lichtfouse, C. Wang, *Environ. Chem. Lett.* **2019**, *17*, 629.
[36] P. Tan, Y. Jiang, S.-C. Qi, X.-J. Gao, X.-Q. Liu, L.-B. Sun, *Engineering* **2020**, *6*, 569.
[37] A. Chaix, G. Mouchaham, A. Shkurenko, P. Hoang, B. Moosa, P. M. Bhatt, K. Adil, K. N. Salama, M. Eddaoudi, N. M. Khashab, *J. Am. Chem. Soc.* **2018**, *140*, 14571.
[38] C. Lin, Y. Qiu, J. Fan, M. Wang, L. Ye, Y. Liu, X. Ye, X. Huang, Y. Lv, M. Liu, *Chem. Eng. J.* **2020**, *394*, 124841.
[39] B. Zhang, J. Yan, Z. Wang, *J. Phys. Chem. C* **2018**, *122*, 12831.
[40] Q. Sun, B. Aguila, Y. Song, S. Ma, *Acc. Chem. Res.* **2020**, *53*, 812.
[41] J. Shuyue, T. Dongyan, P. Jing, Y. Xu, S. Zhaojie, *Chem. Eng. J.* **2020**, *390*, 124472.
[42] M. Karmakar, H. Mondal, T. Ghosh, P. K. Chattopadhyay, D. K. Maiti, N. R. Singha, *Environ. Res.* **2019**, *179*, 108839.
[43] L. A. Shah, M. Khan, R. Javed, M. Sayed, M. S. Khan, A. Khan, M. Ullah, *J. Clean. Prod.* **2018**, *201*, 78.
[44] X. Liu, J. Guan, G. Lai, Q. Xu, X. Bai, Z. Wang, S. Cui, *J. Clean. Prod.* **2020**, *253*, 119915.
[45] W. Fu, X. Wang, Z. Huang, *Sci. Total Environ.* **2019**, *659*, 895.
[46] M. E. Peralta, S. Ocampo, I. G. Funes, F. Onaga Medina, M. E. Parolo, L. Carlos, *Inorganics* **2020**, *8*, 24.
[47] J. Liao, H. Huang, *Carbohydr. Polym.* **2019**, *220*, 191.
[48] J. Pang, Y. Chao, H. Chang, H. Li, J. Xiong, Q. Zhang, G. Chen, J. Qian, W. Zhu, H. Li, *ACS Sustainable Chem. Eng.* **2018**, *6*, 4948.
[49] Z. Wang, S. Guo, Z. Wu, H. Fan, G. Guan, X. Hao, *Sep. Purif. Technol.* **2017**, *187*, 199.
[50] N. Ammavasi, R. Mariappan, *J. Environ. Chem. Eng.* **2018**, *6*, 5645.
[51] R. Petrucci, I. Chiarotto, L. Mattiello, D. Passeri, M. Rossi, G. Zollo, M. Feroci, *Molecules* **2019**, *24*, 4247.
[52] K. Hayashi, T. Matsuyama, J. Ida, *Powder Technol.* **2019**, *355*, 183.
[53] J. Li, Q. Zhou, Y. Wu, Y. Yuan, Y. Liu, *Chemosphere* **2018**, *195*, 472.
[54] J. Jeevanandam, Y. S. Chan, M. K. Danquah, *ChemistrySelect* **2017**, *2*, 10393.
[55] S. Bhatia, N. Verma, R. Kumar, *J. Alloys Compd.* **2017**, *726*, 1274.
[56] B. Wang, W. Liu, W. Zhang, J. Liu, *Nano Res.* **2017**, *10*, 3826.
[57] M. Talukdar, S. K. Behera, P. Deb, *Dalt. Trans.* **2019**, *48*, 12137.
[58] Y. Yurekli, *J. Hazard. Mater.* **2019**, *378*, 120743.
[59] A. Afkhami, R. Moosavi, *J. Hazard. Mater.* **2010**, *174*, 398.
[60] X. Hao, S. Chen, D. Qin, M. Zhang, W. Li, J. Fan, C. Wang, M. Dong, J. Zhang, F. Cheng, Z. Guo, *Mater. Sci. Eng. C* **2020**, *108*, 110361.
[61] Z. Bai, Q. Liu, H. Zhang, J. Liu, J. Yu, J. Wang, *Chem. Eng. J.* **2020**, *382*, 122555.
[62] Q. Yu, Y. Yuan, J. Wen, X. Zhao, S. Zhao, D. Wang, C. Li, X. Wang, N. Wang, *Adv. Sci.* **2019**, *6*, 1900002.
[63] J. Li, R. Wang, D. Zhang, Z. Su, H. Li, Y. Yan, *J. Alloys Compd.* **2019**, *774*, 191.
[64] Y. Shen, C. Zhu, S. Song, T. Zeng, L. Li, Z. Cai, *Environ. Sci. Technol.* **2019**, *53*, 9091.
[65] N. Li, G. Chen, J. Zhao, B. Yan, Z. Cheng, L. Meng, V. Chen, *J. Memb. Sci.* **2019**, *591*, 117341.
[66] S. Li, J. Xu, G. Yao, H. Liu, *Ind. Eng. Chem. Res.* **2019**, *58*, 17075.
[67] L. Han, Y. He, R. An, X. Wang, Y. Zhang, L. Shi, R. Ran, *Colloids Surfaces A Physicochem. Eng. Asp.* **2019**, *569*, 18.
[68] S. Ren, P. Sun, A. Wu, N. Sun, L. Sun, B. Dong, L. Zheng, *New J. Chem.* **2019**, *43*, 7701.
[69] E. Shchukina, H. Wang, D. G. Shchukin, *Chem. Commun.* **2019**, *55*, 3859.
[70] M. Kuddushi, J. Mata, N. Malek, *J. Mol. Liq.* **2020**, *298*, 112048.
[71] T. Xiang, T. Lu, W.-F. Zhao, C.-S. Zhao, *Langmuir* **2019**, *35*, 1146.
[72] S. Sarkar, S. Dutta, P. Bairi, T. Pal, *Langmuir* **2014**, *30*, 7833.
[73] W. Lee, D. Kim, S. Lee, J. Park, S. Oh, G. Kim, J. Lim, J. Kim, *Nano Today* **2018**, *23*, 97.
[74] Y. J. Kim, Y. T. Matsunaga, *J. Mater. Chem. B* **2017**, *5*, 4307.
[75] A. Bordat, T. Boissenot, J. Nicolas, N. Tsapis, *Adv. Drug Delivery Rev.* **2019**, *138*, 167.
[76] P. Makvandi, G. W. Ali, F. Della Sala, W. I. Abdel-Fattah, A. Borzacchiello, *Carbohydr. Polym.* **2019**, *223*, 115023.
[77] A. Gandhi, A. Paul, S. O. Sen, K. K. Sen, *Asian J. Pharm. Sci.* **2015**, *10*, 99.
[78] F. Doberenz, K. Zeng, C. Willems, K. Zhang, T. Groth, *J. Mater. Chem. B* **2020**, *8*, 607.
[79] N. A. Cortez-Lemus, A. Licea-Claverie, *Prog. Polym. Sci.* **2016**, *53*, 1.
[80] K. Nagase, T. Okano, *J. Mater. Chem. B* **2016**, *4*, 6381.
[81] J. J. Ding, J. Zhu, Y. X. Li, X. Q. Liu, L. B. Sun, *Ind. Eng. Chem. Res.* **2017**, *56*, 4341.
[82] S. Gong, T. He, Q. Huang, X. Shu, X. Zhou, *SN Appl. Sci.* **2020**, *2*, 825.
[83] Y. Jiang, S. F. Shan, W. Liu, J. Zhu, Q. X. He, P. Tan, L. Cheng, X. Q. Liu, L. B. Sun, *Chem. Commun.* **2017**, *53*, 9538.
[84] P. Makvandi, G. W. Ali, F. Della Sala, W. I. Abdel-Fattah, A. Borzacchiello, *Mater. Sci. Eng. C* **2019**, *107*, 10195.
[85] K. Yanase, R. Buchner, T. Sato, *J. Mol. Liq.* **2020**, *302*, 112025.
[86] J. J. Chen, A. L. Ahmad, J. K. Lim, B. S. Ooi, *Mater. Chem. Phys.* **2018**, *218*, 39.
[87] R. Dong, J. Li, H. Xiong, W. Lu, H. Peng, L. Chen, *Talanta* **2014**, *130*, 182.
[88] X. Li, B. Zhang, W. Li, X. Lei, X. Fan, L. Tian, H. Zhang, Q. Zhang, *Biosens. Bioelectron.* **2014**, *51*, 261.
[89] A. Halperin, M. Kröger, F. M. Winnik, *Angew. Chem. Int. Ed.* **2015**, *54*, 15342.
[90] M. F. X. Lee, E. S. Chan, K. C. Tam, B. T. Tey, *J. Chromatogr. A* **2015**, *1394*, 71.
[91] Y. Guo, X. Zhang, X. Sun, D. Kong, M. Han, X. Wang, *ACS Omega* **2019**, *4*, 14162.
[92] F. Pishgar, H. Ahmad Panahi, A. A. Khodaparast Haghi, V. Motaghitalab, A. H. Hasani, *J. Chem.* **2016**, *2016*, 8329650.
[93] Z. Gong, S. Li, J. Ma, X. Zhang, *Sep. Purif. Technol.* **2016**, *157*, 131.
[94] M. Liu, Y. Wen, X. Song, J. L. Zhu, J. Li, *Carbohydr. Polym.* **2019**, *219*, 280.
[95] A. Nakamura, K. Sugawara, S. Nakajima, K. Murakami, *Colloids Surfaces A Physicochem. Eng. Asp.* **2017**, *527*, 63.
[96] G. R. Deen, Z. L. Lim, C. H. Mah, S. Q. Tng, M. Sakthivel, Y. Q. Lim, X. J. Loh, *Sep. Sci. Technol.* **2015**, *50*, 64.

© 2021 Wiley-VCH GmbH

[97] X. J. Ju, S. B. Zhang, M. Y. Zhou, R. Xie, L. Yang, L. Y. Chu, *J. Hazard. Mater.* **2009**, *167*, 114.
[98] B. Yang, D. Xu, X. Wu, Z. Li, L. Lei, X. Zhang, *J. Ind. Eng. Chem.* **2015**, *25*, 67.
[99] Y. Jiang, P. Tan, L. Cheng, S.-F. Shan, X.-Q. Liu, L.-B. Sun, *Phys. Chem. Chem. Phys.* **2016**, *18*, 9883.
[100] Y. Liu, R. Chen, D. Yuan, Z. Liu, M. Meng, Y. Wang, J. Han, X. Meng, F. Liu, Z. Hu, W. Guo, L. Ni, Y. Yan, *Colloid Polym. Sci.* **2015**, *293*, 109.
[101] Z. Si, P. Yu, Y. Dong, Y. Lu, Z. Tan, X. Yu, R. Zhao, Y. Yan, *Front. Chem.* **2019**, *6*, 674.
[102] Y. Li, H. Xiao, Y. Pan, M. Zhang, S. Ni, X. Hou, E. Hu, *J. Environ. Manage.* **2018**, *228*, 85.
[103] F. Yan, M. Wang, D. Cao, S. Guo, L. Chen, *J. Polym. Sci. Part A Polym. Chem.* **2013**, *51*, 2401.
[104] N. Tizro, E. Moniri, K. Saeb, H. A. Panahi, S. S. Ardakani, *Microchem. J.* **2019**, *145*, 59.
[105] M. Luzon, T. Corrales, *J. Therm. Anal. Calorim.* **2014**, *116*, 401.
[106] K. R. Shoueir, A. Sarhan, A. M. Atta, M. A. Akl, *Sep. Sci. Technol.* **2016**, *51*, 1605.
[107] W. Liu, L. Qin, Z. An, L. Chen, X. Liu, Y. Yang, B. Xu, *Environ. Chem.* **2018**, *15*, 306.
[108] Z. Li, H. Tian, Y. Yuan, X. Yin, X. Wei, L. Tang, S. Wei, *J. Mater. Chem. A* **2019**, *7*, 11742.
[109] M. Zhang, Y. Li, Q. Yang, L. Huang, L. Chen, Y. Ni, H. Xiao, *Carbohydr. Polym.* **2018**, *195*, 495.
[110] Y. S. Kim, H. M. Lee, J. H. Kim, J. Joo, I. W. Cheong, *RSC Adv.* **2015**, *5*, 10656.
[111] J. Tan, S. Xie, G. Wang, C. W. Yu, T. Zeng, P. Cai, H. Huang, *Polymers (Basel)* **2020**, *12*, 151.
[112] Y. Xie, W. Huang, B. Zheng, S. Li, Q. Liu, Z. Chen, W. Mai, R. Fu, D. Wu, *Adv. Mater.* **2019**, *31*, 1900104.
[113] J. Zhu, P. Tan, P.-P. Yang, X.-Q. Liu, Y. Jiang, L.-B. Sun, *Chem. Commun.* **2016**, *52*, 11531.
[114] P. K. Kundu, D. Samanta, R. Leizrowice, B. Margulis, H. Zhao, M. Börner, T. Udayabhaskararao, D. Manna, R. Klajn, *Nat. Chem.* **2015**, *7*, 646.
[115] D. Brühwiler, *Nanoscale* **2010**, *2*, 887.
[116] N. Huang, X. Ding, J. Kim, H. Ihee, D. Jiang, *Angew. Chem.* **2015**, *127*, 8828.
[117] L. Zhao, D. A. Loy, K. J. Shea, *J. Am. Chem. Soc.* **2006**, *128*, 14250.
[118] Y. Mao, Q. Wang, L. Yu, H. Qian, S. Deng, W. Xiao, D. Zhao, C. Chen, *Inorg. Chem.* **2020**, *59*, 8213.
[119] M. Wen, G. Li, H. Liu, J. Chen, T. An, H. Yamashita, *Environ. Sci. Nano* **2019**, *6*, 1006.
[120] B. Li, Q. Sun, Y. Zhang, C. W. Abney, B. Aguila, W. Lin, S. Ma, *ACS Appl. Mater. Interfaces* **2017**, *9*, 12511.
[121] R. Zhao, T. Ma, S. Li, Y. Tian, G. Zhu, *ACS Appl. Mater. Interfaces* **2019**, *11*, 16662.
[122] W. Zhou, Z. Qiao, E. Nazarzadeh Zare, J. Huang, X. Zheng, X. Sun, M. Shao, H. Wang, X. Wang, D. Chen, J. Zheng, S. Fang, Y. M. Li, X. Zhang, L. Yang, P. Makvandi, A. Wu, *J. Med. Chem.* **2020**, *63*, 8003.
[123] J. W. Brown, B. L. Henderson, M. D. Kiesz, A. C. Whalley, W. Morris, S. Grunder, H. Deng, H. Furukawa, J. I. Zink, J. F. Stoddart, O. M. Yaghi, *Chem. Sci.* **2013**, *4*, 2858.
[124] H. Huang, H. Sato, T. Aida, *J. Am. Chem. Soc.* **2017**, *139*, 8784.
[125] H. Li, M. R. Martinez, Z. Perry, H.-C. Zhou, P. Falcaro, C. Doblin, S. Lim, A. J. Hill, B. Halstead, M. R. Hill, *Chem.– A Eur. J.* **2016**, *22*, 11176.
[126] L. Le Gong, X. F. Feng, F. Luo, *Inorg. Chem.* **2015**, *54*, 11587.
[127] H. M. D. Bandara, S. C. Burdette, *Chem. Soc. Rev.* **2012**, *41*, 1809.
[128] N. Liu, K. Yu, B. Smarsly, D. R. Dunphy, Y.-B. Jiang, C. J. Brinker, *J. Am. Chem. Soc.* **2002**, *124*, 14540.
[129] D. Manna, T. Udayabhaskararao, H. Zhao, R. Klajn, *Angew. Chemie* **2015**, *127*, 12571.
[130] J. Park, D. Yuan, K. T. Pham, J.-R. Li, A. Yakovenko, H.-C. Zhou, *J. Am. Chem. Soc.* **2012**, *134*, 99.
[131] M. Alvaro, M. Benitez, D. Das, H. Garcia, E. Peris, *Chem. Mater.* **2005**, *17*, 4958.
[132] N. Liu, Z. Chen, D. R. Dunphy, Y.-B. Jiang, R. A. Assink, C. J. Brinker, *Angew. Chem., Int. Ed.* **2003**, *42*, 1731.
[133] H. Awala, J.-P. Gilson, R. Retoux, P. Boullay, J.-M. Goupil, V. Valtchev, S. Mintova, *Nat. Mater.* **2015**, *14*, 447.
[134] L. T. Gibson, *Chem. Soc. Rev.* **2014**, *43*, 5173.
[135] W. Li, D. Zhao, *Chem. Commun.* **2013**, *49*, 943.
[136] L. Cheng, Y. Jiang, N. Yan, S.-F. Shan, X.-Q. Liu, L.-B. Sun, *ACS Appl. Mater. Interfaces* **2016**, *8*, 23404.
[137] X. Guan, S. Yan, J. Chang, G. Yang, H. Fan, *Chem. Commun.* **2018**, *54*, 12770.
[138] H. P. C. van Kuringen, Z. J. W. A. Leijten, A. H. Gelebart, D. J. Mulder, G. Portale, D. J. Broer, A. P. H. J. Schenning, *Macromolecules* **2015**, *48*, 4073.
[139] G. Kocak, C. Tuncer, V. Bütün, *Polym. Chem.* **2017**, *8*, 144.
[140] D. Chen, Y. Liu, Y. Qin, L. Wang, Y. Ma, W. Yang, *Chinese J. Chem.* **2017**, *35*, 596.
[141] J. N. Hiremath, B. Vishalakshi, *Polym. Bull.* **2015**, *72*, 3063.
[142] G. Yao, W. Bi, H. Liu, *Colloids Surfaces A Physicochem. Eng. Asp.* **2020**, *588*, 124393.
[143] J. Wolska, M. Kujawska, P. Cyganowski, *Sep. Sci. Technol.* **2020**, *55*, 2137.
[144] Y. Qin, L. Wang, C. Zhao, D. Chen, Y. Ma, W. Yang, *ACS Appl. Mater. Interfaces* **2016**, *8*, 16690.
[145] W. Liu, R. Hu, Y. Li, Y. Huang, Y. Wang, Z. Wei, E. Yu, X. Guo, *RSC Adv.* **2020**, *10*, 4232.
[146] T. Kuroiwa, H. Takada, A. Shogen, K. Saito, I. Kobayashi, K. Uemura, A. Kanazawa, *Colloids Surfaces A Physicochem. Eng. Asp.* **2017**, *514*, 69.
[147] W. Liu, J. Ma, C. Shen, Y. Wen, W. Liu, *Water Res.* **2016**, *90*, 24.
[148] G. Sharma, A. Kumar, S. Sharma, M. Naushad, A. A. Ghfar, H. Ala'a, T. Ahamad, N. Sharma, F. J. Stadler, *Cellulose* **2020**, *27*, 3677.
[149] L. Dong, C. Wen, Y. Junxia, D. Yigang, *J. Dispers. Sci. Technol.* **2017**, *38*, 1832.
[150] J. Ray, S. Jana, S. K. Bhanja, T. Tripathy, *Colloid Polym. Sci.* **2018**, *296*, 1275.
[151] W. Wang, J. Hu, R. Zhang, C. Yan, L. Cui, J. Zhu, *Cellulose* **2020**, *10*, 1.
[152] B. Qiu, J. Guo, X. Zhang, D. Sun, H. Gu, Q. Wang, H. Wang, X. Wang, X. Zhang, B. L. Weeks, *ACS Appl. Mater. Interfaces* **2014**, *6*, 19816.
[153] D. Majhi, B. N. Patra, *RSC Adv.* **2020**, *10*, 43904.
[154] C. Sansuk, S. Phetrong, P. Paoprasert, *Polym. Int.* **2017**, *66*, 787.
[155] S. Liu, Y. Ma, L. Gao, J. Pan, *Chem. Eng. J.* **2018**, *341*, 198.
[156] I. M. El-Nahhal, A. A. A. Shawesh, F. S. Kodeh, S. Kuhn, R. Hempelmann, *J. Sol-Gel Sci. Technol.* **2016**, *77*, 386.
[157] K. A. McDonald, J. I. Feldblyum, K. Koh, A. G. Wong-Foy, A. J. Matzger, *Chem. Commun.* **2015**, *51*, 11994.
[158] S. Liu, J. Pan, J. Cao, X. Dai, M. Meng, R. Wu, J. Yao, Y. Yan, *Chem. Eng. J.* **2016**, *284*, 10.
[159] K. K. Sharma, T. Asefa, *Angew. Chem., Int. Ed.* **2007**, *46*, 2879.
[160] G. E. Fryxell, J. Liu, T. A. Hauser, Z. Nie, K. F. Ferris, S. Mattigod, M. Gong, R. T. Hallen, *Chem. Mater.* **1999**, *11*, 2148.
[161] S. Moosavi, C. W. Lai, S. Gan, G. Zamiri, O. A. Pivehzhani, M. R. Johan, *ACS Omega* **2020**, *5*, 20684.
[162] O. V. Kharissova, H. V. R. Dias, B. I. Kharisov, *RSC Adv.* **2015**, *5*, 6695.
[163] M. T. Siddiqui, S. Nizamuddin, H. A. Baloch, N. M. Mubarak, M. Al-Ali, S. A. Mazari, A. Bhutto, R. Abro, M. Srinivasan, G. Griffin, *J. Environ. Chem. Eng.* **2019**, *7*, 102812.

© 2021 Wiley-VCH GmbH

[164] A. I. Adeogun, *Part. Sci. Technol.* **2020**, *38*, 756.
[165] C. Saucier, P. Karthickeyan, V. Ranjithkumar, E. C. Lima, G. S. dos Reis, I. A. S. de Brum, *Environ. Sci. Pollut. Res.* **2017**, *24*, 5918.
[166] A. C. Fröhlich, E. L. Foletto, G. L. Dotto, *J. Clean. Prod.* **2019**, *229*, 828.
[167] L. S. Rocha, D. Pereira, É. Sousa, M. Otero, V. I. Esteves, V. Calisto, *Sci. Total Environ.* **2020**, *718*, 137272.
[168] B. Kakavandi, M. Jahangiri-Rad, M. Rafiee, A. R. Esfahani, A. A. Babaei, *Microporous Mesoporous Mater.* **2016**, *231*, 192.
[169] K. M. Lompe, S. Vo Duy, S. Peldszus, S. Sauvé, B. Barbeau, *J. Hazard. Mater.* **2018**, *360*, 349.
[170] S. Amornwutiroj, P. Manpetch, W. Singhapong, P. Srinophakun, A. Jaroenworaluck, *J. Dispers. Sci. Technol.* **2020**, *41*, 1427.
[171] M. Baghdadi, E. Ghaffari, B. Aminzadeh, *J. Environ. Chem. Eng.* **2016**, *4*, 3309.
[172] Y. Wang, Z. Xue, X. Zheng, D. Lu, S. Li, X. Li, *Miner. Eng.* **2019**, *139*, 105866.
[173] D. Pereira, L. S. Rocha, M. V. Gil, M. Otero, N. J. O. Silva, V. I. Esteves, V. Calisto, *Environ. Sci. Pollut. Res.* **2020**, *28*, 18314.
[174] P. Yu, X. Li, X. Zhang, H. Zhou, Y. Xu, Y. Sun, H. Zheng, *Sep. Purif. Technol.* **2021**, *254*, 117662.
[175] Z. Hao, C. Wang, Z. Yan, H. Jiang, H. Xu, *Chemosphere* **2018**, *211*, 962.
[176] R. S. Juang, Y. C. Yei, C. S. Liao, K. S. Lin, H. C. Lu, S. F. Wang, A. C. Sun, *J. Taiwan Inst. Chem. Eng.* **2018**, *90*, 51.
[177] L. Sellaoui, E. C. Lima, G. L. Dotto, A. Ben Lamine, *J. Mol. Liq.* **2017**, *234*, 375.
[178] F. Qian, X. Zhu, Y. Liu, S. Hao, Z. J. Ren, B. Gao, R. Zong, S. Zhang, J. Chen, *J. Mater. Chem. A* **2016**, *4*, 18942.
[179] B. Wang, Y. song Jiang, F. yun Li, D. yue Yang, *Bioresour. Technol.* **2017**, *233*, 159.
[180] K. Jung, B. Hyun, K. Guen, J. Choi, *Chemosphere* **2019**, *215*, 432.
[181] S. Zeng, Y. K. Choi, E. Kan, *Sci. Total Environ.* **2021**, *750*, 141691.
[182] H. Ebadollahzadeh, M. Zabihi, *Mater. Chem. Phys.* **2020**, *248*, 122893.
[183] K. Chen, Z. Zhang, K. Xia, X. Zhou, Y. Guo, T. Huang, *ACS Omega* **2019**, *4*, 8568.
[184] D. Bhatia, S. Batra, D. Datta, *Water Sci. Technol.* **2019**, *79*, 1755.
[185] H. Haham, J. Grinblat, M. T. Sougrati, L. Stievano, S. Margel, *Materials (Basel)* **2015**, *8*, 4593.
[186] Y. Li, Y. Zhai, P. Zhang, X. Wang, H. Cui, J. Li, L. Liu, H. Zhao, J. Song, *Colloids Surfaces A Physicochem. Eng. Asp.* **2019**, *563*, 141.
[187] Z. Wu, X. He, Z. Gao, Y. Xue, X. Chen, L. Zhang, *Environ. Sci. Pollut. Res.* **2020**, *28*, 3475.
[188] S. Jorfi, B. Kakavandi, H. R. Motlagh, M. Ahmadi, N. Jaafarzadeh, *Appl. Catal. B Environ.* **2017**, *219*, 216.
[189] B. Kakavandi, N. Bahari, R. Rezaei Kalantary, E. Dehghani Fard, *Ultrason. Sonochem.* **2019**, *55*, 75.
[190] B. Xiong, N. Wang, Y. Chen, H. Peng, *J. Appl. Polym. Sci.* **2018**, *135*, 45876.
[191] A. M. Atta, H. A. Al-Lohedan, A. M. Tawfeek, M. A. Ahmed, *Polym. Int.* **2018**, *67*, 925.
[192] M. Hayasi, N. Saadatjoo, *Adv. Polym. Technol.* **2018**, *37*, 1941.
[193] Y. Cui, W. Kang, L. Qin, J. Ma, X. Liu, Y. Yang, *Chem. Eng. J.* **2020**, *397*, 125480.
[194] L. Qiu, G. Jaria, M. V. Gil, J. Feng, Y. Dai, V. I. Esteves, M. Otero, V. Calisto, *Polymers (Basel).* **2020**, *12*, 1385.
[195] L. Fang, Y. Miao, D. Wei, Y. Zhang, Y. Zhou, *Chemosphere* **2021**, *262*, 128032.
[196] Z. Falahian, F. Torki, H. Faghihian, *Glob. Challenges* **2018**, *2*, 1700078.
[197] T. Ahamad, M. Naushad, S. M. Alshehri, *J. Water Process Eng.* **2020**, *36*, 101284.
[198] P. Arabkhani, A. Asfaram, *J. Hazard. Mater.* **2020**, *384*, 121394.
[199] Z. Lian, Y. Li, H. Xian, X. kun Ouyang, Y. Lu, X. Peng, D. Hu, *Int. J. Biol. Macromol.* **2020**, *165*, 591.
[200] A. Karamipour, P. Khadiv Parsi, P. Zahedi, S. M. A. Moosavian, *Int. J. Biol. Macromol.* **2020**, *154*, 1132.
[201] L. P. Lingamdinne, J. R. Koduru, R. R. Karri, *J. Environ. Manage.* **2019**, *231*, 622.
[202] X. Wan, Y. Huang, Y. Chen, *Acc. Chem. Res.* **2012**, *45*, 598.
[203] L. P. Lingamdinne, S. Lee, J. S. Choi, V. R. Lebaka, V. R. P. Durbaka, J. R. Koduru, *J. Hazard. Mater.* **2021**, *402*, 123882.
[204] M. Adel, M. A. Ahmed, A. A. Mohamed, *Compos. Commun.* **2020**, *22*, 100450.
[205] J. Xiong, D. Zhang, H. Lin, Y. Chen, *Chem. Eng. J.* **2020**, *400*, 125890.
[206] N. A. Elessawy, M. Elnouby, M. H. Gouda, H. A. Hamad, N. A. Taha, M. Gouda, M. S. Mohy Eldin, *Chemosphere* **2020**, *239*, 124728.
[207] S. Saber-Samandari, S. Saber-Samandari, H. Joneidi-Yekta, M. Mohseni, *Chem. Eng. J.* **2017**, *308*, 1133.
[208] L. Fan, A. Zhou, L. Zhong, Z. Zhang, Y. Liu, *Chemosphere* **2019**, *226*, 405.
[209] S. M. Wabaidur, M. A. Khan, M. R. Siddiqui, M. Otero, B. H. Jeon, Z. A. Alothman, A. A. H. Hakami, *J. Mol. Liq.* **2020**, *317*, 113916.
[210] E. I. Nosike, Z. Jiang, L. Miao, O. U. Akakuru, B. Yuan, S. Wu, Y. Zhang, Y. Zhang, A. Wu, *J. Hazard. Mater.* **2020**, *392*, 122288.
[211] H. Duan, X. Hu, Z. Sun, *J. Hazard. Mater.* **2020**, *384*, 121406.
[212] E. C. Paris, J. O. D. Malafatti, H. C. Musetti, A. Manzoli, A. Zenatti, M. T. Escote, *Chinese J. Chem. Eng.* **2020**, *28*, 1884.
[213] C. Ye, P. Lu, X. Jiang, C. Wu, T. Qiu, Y. Li, *Chem. Eng. Process. – Process Intensif.* **2020**, *153*, 107961.
[214] M. Khatamian, N. Khodakarampoor, M. Saket-Oskoui, *J. Colloid Interface Sci.* **2017**, *498*, 433.
[215] M. Brigante, E. Pecini, M. Avena, *Microporous Mesoporous Mater.* **2016**, *230*, 1.
[216] X. Zhang, Y. Zhang, X. Zhang, S. Li, Y. Huang, *J. Hazard. Mater.* **2017**, *337*, 1.
[217] P. Xu, Z. Nan, *Mater. Lett.* **2018**, *218*, 209.
[218] H. He, X. Meng, Q. Yue, W. Yin, Y. Gao, P. Fang, L. Shen, *Chem. Eng. J.* **2021**, *405*, 126743.
[219] X. Guan, S. Yan, D. Hou, H. Fan, *Chem. Phys. Lett.* **2019**, *714*, 11.
[220] Y. Liang, H. Zhu, L. Wang, H. He, S. Wang, *Carbohydr. Polym.* **2020**, *249*, 116876.
[221] J. S. Karthika, B. Vishalakshi, *Int. J. Biol. Macromol.* **2015**, *81*, 648.
[222] G. Yao, S. Li, J. Xu, H. Liu, *J. Chem. Eng. Data* **2019**, *64*, 4054.
[223] Y. Zhen, Z. Ning, Z. Shaopeng, D. Yayi, Z. Xuntong, S. Jiachun, Y. Weiben, W. Yuping, C. Jianqiang, *ACS Appl. Mater. Interfaces* **2015**, *7*, 24446.
[224] S. Ganta, D. K. Chand, *Inorg. Chem.* **2018**, *57*, 3634.
[225] L. Yan, M. Lv, C. Su, L. Zheng, J. Li, Z. Ye, *Soft Matter* **2017**, *13*, 8772.
[226] P. Tabrizian, W. Ma, A. Bakr, M. S. Rahaman, *J. Colloid Interface Sci.* **2019**, *534*, 549.
[227] J. Cheng, G. Shan, P. Pan, *RSC Adv.* **2015**, *5*, 62091.
[228] Y. Zhong, X. Wang, Z. Zheng, P. Du, *J. Appl. Polym. Sci.* **2015**, *132*, 41944.
[229] J. Cheng, G. Shan, P. Pan, *Ind. Eng. Chem. Res.* **2017**, *56*, 1223.
[230] L.-H. Qi, J.-D. Ding, X.-Q. Ma, X.-W. Guan, W. Zhu, H. Yao, Y.-M. Zhang, T.-B. Wei, Q. Lin, *Soft Matter* **2019**, *15*, 6836.
[231] E. G. Vlakh, V. A. Korzhikov, A. V Hubina, T. B. Tennikova, *Russ. Chem. Rev.* **2015**, *84*, 952.
[232] B. Ram, G. S. Chauhan, *Chem. Eng. J.* **2018**, *331*, 587.
[233] S. R. Thakare, M. R. Pal, S. Z. Jadhao, *Des. Monomers Polym.* **2015**, *18*, 650.
[234] F. S. Awad, K. M. AbouZeid, W. M. A. El-Maaty, A. M. El-Wakil, M. S. El-Shall, *ACS Appl. Mater. Interfaces* **2017**, *9*, 34230.
[235] Z. Su, H. Zhang, Y. Gao, L. Huo, Y. Wu, X. Ba, *Chem. Eng. J.* **2020**, *393*, 124695.

© 2021 Wiley-VCH GmbH

[236] B. A. Omondi, H. Okabe, Y. Hidaka, K. Hara, *React. Funct. Polym.* **2018**, *125*, 11.
[237] D. T. Sun, L. Peng, W. S. Reeder, S. M. Moosavi, D. Tiana, D. K. Britt, E. Oveisi, W. L. Queen, *ACS Cent. Sci.* **2018**, *4*, 349.
[238] S. Chatterjee, N. Guha, S. Krishnan, A. K. Singh, P. Mathur, D. K. Rai, *Sci. Rep.* **2020**, *10*, 1.
[239] A. S. Ogunlaja, C. Du Sautoy, N. Torto, Z. R. Tshentu, *Talanta* **2014**, *126*, 61.
[240] X. Yuan, C. Zhang, M. Xie, X. Li, *Colloids Surfaces A Physicochem. Eng. Asp.* **2020**, *586*, 124235.
[241] C. Huang, X. Shi, C. Wang, L. Guo, M. Dong, G. Hu, J. Lin, T. Ding, Z. Guo, *Int. J. Biol. Macromol.* **2019**, *140*, 1167.
[242] Y. Huang, R. Wang, *Chem. Eng. J.* **2019**, *378*, 122084.
[243] H. Molavi, A. Hakimian, A. Shojaei, M. Raeiszadeh, *Appl. Surf. Sci.* **2018**, *445*, 424.
[244] T. H. Bui, W. Lee, S.-B. Jeon, K.-W. Kim, Y. Lee, *Sep. Purif. Technol.* **2020**, *248*, 116989.
[245] F. Yuan, C. Wu, Y. Cai, L. Zhang, J. Wang, L. Chen, X. Wang, S. Yang, S. Wang, *Chem. Eng. J.* **2017**, *322*, 353.
[246] L. M. Madikizela, L. Chimuka, *J. Environ. Chem. Eng.* **2016**, *4*, 4029.
[247] J. Liu, J. Pan, Y. Ma, S. Liu, F. Qiu, Y. Yan, *Chem. Eng. J.* **2018**, *332*, 517.
[248] H. Ju, X. Zhou, B. Shi, X. Kong, H. Xing, F. Huang, *Polym. Chem.* **2019**, *10*, 5821.
[249] K. Dwivedi, A. Morone, T. Chakrabarti, R. A. Pandey, *J. Environ. Chem. Eng.* **2018**, *6*, 3681.
[250] D. Babilas, P. Dydo, *Sep. Sci. Technol.* **2019**, *55*, 2250.
[251] Y. Deng, Y. Xiao, Y. Zhou, T. Zeng, M. Xing, J. Zhang, *Catal. Today* **2019**, *335*, 101.
[252] Y. Tang, J. Zhao, J. Zhou, Y. Zeng, W. Zhang, B. Shi, *Water Res.* **2020**, *178*, 115807.
[253] K. Z. Elwakeel, A. A. El-Bindary, E. Y. Kouta, E. Guibal, *Chem. Eng. J.* **2018**, *332*, 727.
[254] H. Wu, Z. Liu, A. Li, H. Yang, *Chemosphere* **2017**, *174*, 200.
[255] Y. Verkh, M. Rozman, M. Petrovic, *Chemosphere* **2018**, *200*, 397.
[256] P. Verlicchi, M. Al Aukidy, A. Galletti, M. Petrovic, D. Barceló, *Sci. Total Environ.* **2012**, *430*, 109.
[257] V. S. Thomaidi, A. S. Stasinakis, V. L. Borova, N. S. Thomaidis, *J. Hazard. Mater.* **2015**, *283*, 740.
[258] S. Mohan, P. Balakrishnan, *Water, Air, Soil Pollut.* **2019**, *230*, 69.
[259] T. S. Oliveira, M. Murphy, N. Mendola, V. Wong, D. Carlson, L. Waring, *Sci. Total Environ.* **2015**, *518–519*, 459.
[260] Z. Hao, L. Chen, C. Wang, X. Zou, F. Zheng, W. Feng, D. Zhang, L. Peng, *Chemosphere* **2019**, *226*, 340.
[261] Z. Cheng, C.-L. Lam, W.-Y. Mo, X.-P. Nie, W.-M. Choi, Y.-B. Man, M.-H. Wong, *Environ. Sci. Pollut. Res.* **2016**, *23*, 7195.
[262] J.-H. Kim, J.-C. Kang, *Chemosphere* **2017**, *176*, 131.
[263] E. Goretti, M. Pallottini, M. I. Ricciarini, R. Selvaggi, D. Cappelletti, *Sci. Total Environ.* **2016**, *559*, 339.
[264] B. Clasen, V. L. Loro, C. R. Murussi, T. L. Tiecher, B. Moraes, R. Zanella, *Sci. Total Environ.* **2018**, *626*, 737.
[265] A. Buah-Kwofie, M. S. Humphries, L. Pillay, *Sci. Total Environ.* **2018**, *621*, 273.
[266] M. A. de Boer, M. Hammerton, J. C. Slootweg, *Water Res.* **2018**, *133*, 19.
[267] A. Anwar-Mohamed, R. H. Elbekai, A. O. S. El-Kadi, *Expert Opin. Drug Metab. Toxicol.* **2009**, *5*, 501.
[268] S. Rajeshkumar, X. Li, *Toxicol. Rep.* **2018**, *5*, 288.
[269] C. T. Vu, C. Lin, G. Yeh, M. C. Villanueva, *Environ. Sci. Pollut. Res.* **2017**, *24*, 19422.
[270] S. S. Bhatti, V. Sambyal, J. Singh, A. K. Nagpal, *Environ. Dev. Sustain.* **2017**, *19*, 571.
[271] M. Huertas, L. López-Maury, J. Giner-Lamia, A. Sánchez-Riego, F. Florencio, *Life* **2014**, *4*, 865.
[272] M. Oves, M. S. Khan, H. A. Qari, *J. Taiwan Inst. Chem. Eng.* **2017**, *80*, 540.
[273] S. Bhatti, G. N. V. Satyanarayana, D. K. Patel, A. Satish, *Chemosphere* **2019**, *231*, 207.
[274] T. S. Oliveira, M. Al Aukidy, P. Verlicchi, in *The Handbook of Environmental Chemistry*, Springer, Berlin **2017**, pp. 17–32.
[275] O. Miarov, A. Tal, D. Avisar, *J. Environ. Manage.* **2020**, *254*, 109794.
[276] E. Carraro, S. Bonetta, C. Bertino, E. Lorenzi, S. Bonetta, G. Gilli, *J. Environ. Manage.* **2016**, *168*, 185.
[277] P. Suresh Kumar, W. W. Ejerssa, C. C. Wegener, L. Korving, A. I. Dugulan, H. Temmink, M. C. M. van Loosdrecht, G.-J. Witkamp, *Water Res.* **2018**, *145*, 365.
[278] M. Vakili, S. Deng, G. Cagnetta, W. Wang, P. Meng, D. Liu, G. Yu, *Sep. Purif. Technol.* **2019**, *224*, 373.
[279] H. Shemer, A. Armush, R. Semiat, *Colloids Surfaces A Physicochem. Eng. Asp.* **2019**, *579*, 123680.
[280] M. Kunaschk, V. Schmalz, N. Dietrich, T. Dittmar, E. Worch, *Water Res.* **2015**, *71*, 219.
[281] Z. N. Garba, W. Zhou, M. Zhang, Z. Yuan, *Chemosphere* **2020**, *244*, 125474.
[282] J. N. Putro, A. Kurniawan, S. Ismadji, Y.-H. Ju, *Environ. Nanotechnology, Monit. Manag.* **2017**, *8*, 134.
[283] M. Hassan, R. Naidu, J. Du, Y. Liu, F. Qi, *Sci. Total Environ.* **2020**, *702*, 134893.
[284] M. A. M. Reshadi, A. Bazargan, G. McKay, *Sci. Total Environ.* **2020**, *731*, 138863.
[285] G. L. Dotto, G. McKay, *J. Environ. Chem. Eng.* **2020**, *8*, 103988.
[286] Momina, M. Shahadat, S. Isamil, *RSC Adv.* **2018**, *8*, 24571.
[287] S. Lata, P. K. Singh, S. R. Samadder, *Int. J. Environ. Sci. Technol.* **2015**, *12*, 1461.
[288] S. Kulkarni, J. Kaware, *Int. J. Innov. Sci. Eng. Technol.* **2014**, *1*, 61.
[289] L. Tang, G. Wang, Z. Zeng, L. Shen, L. Zhu, Y. Zhang, Q. Xue, *J. Colloid Interface Sci.* **2020**, *575*, 231.
[290] Y. Li, X. Hou, Y. Pan, L. Wang, H. Xiao, *Eur. Polym. J.* **2020**, *123*, 109447.
[291] T. A. Saleh, S. A. Haladu, S. A. Ali, *Chem. Eng. J.* **2015**, *269*, 9.
[292] Y. Chen, R. Xu, Y. Li, Y. Liu, Y. Wu, Y. Chen, J. Zhang, S. Chen, H. Yin, Z. Zeng, S. Wang, Z. Peng, *Colloids Surfaces A Physicochem. Eng. Asp.* **2020**, *599*, 124870.
[293] M. Behbahani, Y. Bide, S. Bagheri, M. Salarian, F. Omidi, M. R. Nabid, *Microchim. Acta* **2016**, *183*, 111.
[294] N. Sivagangi Reddy, K. Madhusudana Rao, T. J. Sudha Vani, K. S. V. Krishna Rao, Y. I. Lee, *Desalin. Water Treat.* **2016**, *57*, 6503.
[295] K. A. S. Bornillo, S. Kim, H. Choi, *Chemosphere* **2020**, *242*, 125287.
[296] Y. Liu, X. Hu, Z. Liu, M. Meng, J. Pan, Y. Jiang, L. Ni, W. Wu, *Chem. Eng. J.* **2017**, *328*, 11.
[297] S. A. Ali, I. B. Rachman, T. A. Saleh, *Chem. Eng. J.* **2017**, *330*, 663.
[298] X. Zheng, R. Fan, K. Xing, K. Zhu, P. Wang, Y. Yang, *Chem. Eng. J.* **2020**, *380*, 122580.
[299] B. Xu, H. Zheng, H. Zhou, Y. Wang, K. Luo, C. Zhao, Y. Peng, X. Zheng, *J. Mol. Liq.* **2018**, *256*, 424.
[300] F. M. Valadi, A. Ekramipooya, M. R. Gholami, *J. Mol. Liq.* **2020**, *318*, 114051.
[301] H. S. Alaei, M. S. Tehrani, S. W. Husain, H. A. Panahi, A. Mehramizi, *React. Funct. Polym.* **2019**, *136*, 58.
[302] K. Yu, D. Wang, Q. Wang, *Polymers (Basel)*. **2018**, *10*, 880.
[303] A. Ma, G. Wang, Z. Yang, L. Bai, H. Chen, W. Wang, H. Yang, D. Wei, L. Yang, *Chem. Eng. J.* **2020**, *385*, 123962.
[304] W. Cui, J. Ji, Y.-F. Cai, H. Li, R. Ran, *J. Mater. Chem. A* **2015**, *3*, 17445.
[305] Z. Gong, G. Zhang, X. Zeng, J. Li, G. Li, W. Huang, R. Sun, C. Wong, *ACS Appl. Mater. Interfaces* **2016**, *8*, 24030.
[306] C. K. Karan, M. Bhattacharjee, *ACS Appl. Mater. Interfaces* **2016**, *8*, 5526.
[307] J. Liu, W. Duan, J. Song, X. Guo, Z. Wang, X. Shi, J. Liang, J. Wang, P. Cheng, Y. Chen, M. J. Zaworotko, Z. Zhang, *J. Am. Chem. Soc.* **2019**, *141*, 12064.

© 2021 Wiley-VCH GmbH

[308] W. Lu, C. Duan, C. Liu, Y. Zhang, X. Meng, L. Dai, W. Wang, H. Yu, Y. Ni, *Carbohydr. Polym.* **2020**, *247*, 116691.
[309] W. Yao, L. Li, O. L. Li, Y.-W. Cho, M.-Y. Jeong, Y.-R. Cho, *Chem. Eng. J.* **2018**, *352*, 173.
[310] M. S. Khazravi, M. Bahmaei, M. E. Olya, S. M. Etezad, *Prog. Color. Color. Coatings* **2019**, *12*, 39.
[311] A. A. Essawy, S. M. Sayyah, A. M. El-Nggar, *J. Photochem. Photobiol. B Biol.* **2017**, *173*, 170.
[312] Y. Xiong, L. Xu, C. Jin, Q. Sun, *Cellulose* **2020**, *27*, 7751.
[313] C. Pan, L. Liu, Q. Chen, Q. Zhang, G. Guo, *ACS Appl. Mater. Interfaces* **2017**, *9*, 38052.
[314] A. Pettignano, S. Grijalvo, M. Häring, R. Eritja, N. Tanchoux, F. Quignard, D. Díaz Díaz, *Chem. Commun.* **2017**, *53*, 3350.
[315] A. Jilani, S. Z. Hussain, A. A. P. Khan, A. Khan, M. H. D. Othman, M. O. Ansari, in *Self-Healing Composite Materials*, Elsevier, Amsterdam **2020**, pp. 163–175.
[316] A. Sharma, K. Rawat, P. R. Solanki, H. B. Bohidar, *Int. J. Biol. Macromol.* **2017**, *95*, 603.
[317] B. Wang, Y. S. Jeon, H. S. Park, J.-H. Kim, *Mater. Sci. Eng. C* **2016**, *69*, 160.
[318] I. Álvarez-Manzaneda, E. Ramos-Rodríguez, M. J. López-Rodríguez, G. Parra, A. Funes, I. de Vicente, *J. Hazard. Mater.* **2017**, *322*, 437.
[319] F. Côa, M. Strauss, Z. Clemente, L. L. Rodrigues Neto, J. R. Lopes, R. S. Alencar, A. G. Souza Filho, O. L. Alves, V. L. S. S. Castro, E. Barbieri, D. S. T. Martinez, *Sci. Total Environ.* **2017**, *607–608*, 1479.
[320] I. Álvarez-Manzaneda, A. Baun, L. Cruz-Pizarro, I. de Vicente, *Chemosphere* **2019**, *222*, 469.
[321] I. Kozyatnyk, D. M. M. Yacout, J. Van Caneghem, S. Jansson, *Bioresour. Technol.* **2020**, *302*, 122866.
[322] S. P. C. Gonçalves, M. Strauss, F. S. Delite, Z. Clemente, V. L. Castro, D. S. T. Martinez, *Sci. Total Environ.* **2016**, *565*, 833.
[323] L. De Marchi, C. Pretti, B. Gabriel, P. A. A. P. Marques, R. Freitas, V. Neto, *Sci. Total Environ.* **2018**, *631–632*, 1440.
[324] Y.-Q. Zhang, R. Dringen, C. Petters, W. Rastedt, J. Köser, J. Filser, S. Stolte, *Environ. Sci. Nano* **2016**, *3*, 754.
[325] Y. Wang, X. Zhu, Y. Lao, X. Lv, Y. Tao, B. Huang, J. Wang, J. Zhou, Z. Cai, *Sci. Total Environ.* **2016**, *565*, 818.
[326] G. Svartz, M. Papa, M. Gosatti, M. Jordán, A. Soldati, P. Samter, M. M. Guraya, C. Pérez Coll, S. Perez Catán, *Ecotoxicol. Environ. Saf.* **2017**, *144*, 200.

Ehsan Nazarzadeh Zare received his Ph.D. in Polymer Chemistry from the University of Mazandaran, Iran, in 2015. He was a Postdoctoral Research Fellow at the University of Mazandaran from May 2015 to May 2016. Currently, he is an Assistant Professor in Polymer Chemistry at Damghan University, Damghan, Iran. His current research interests include design of novel nanomaterials for biomedical applications, and water treatment.

Ackmez Mudhoo received his B.Eng. (Hons.) degree in Chemical and Environmental Engineering in 2004, Master of Philosophy (M.Phil.) degree in Chemical Engineering in 2011, and Doctor of Philosophy (Ph.D.) degree in Environmental Engineering in 2018, all from the University of Mauritius. He is a Lecturer in the Department of Chemical and Environmental Engineering at the University of Mauritius. His research interests are in chemical process design and analysis, bioremediation of solid residues and wastewaters, and in the depuration of contaminated aqueous media using adsorption-based methods.

© 2021 Wiley-VCH GmbH

Moonis Ali Khan received his Ph.D. degree in Applied Chemistry from Aligarh Muslim University, Aligarh, India, in 2009. From 2009 to 2011, he worked as a Post-Doctoral Researcher at Yonsei University, South Korea, and Universiti Putra Malaysia, Malaysia. Currently, he is working as an Associate Professor in the Chemistry Department at the King Saud University, Riyadh, Saudi Arabia. He is an interfacial chemist, and his research is focused in the synthesis and development of novel materials for environmental remediation applications.

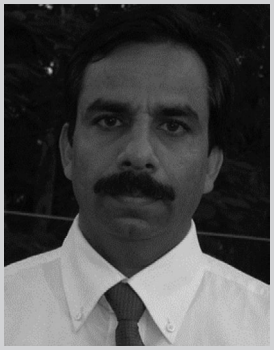

Dinesh Mohan is a Professor in the School of Environmental Sciences at Jawaharlal Nehru University, New Delhi, India. He obtained his Ph.D. degree in 1995 in Chemistry from the Indian Institute of Technology Roorkee, Roorkee, India. He is an Elected Fellow of the Royal Society of Chemistry (FRSC) London and the National Academy of Agricultural Sciences (NAAS). He is also an Adjunct Professor at the Chemistry Department, Mississippi State University, USA. His research areas span groundwater, surface water and wastewater monitoring, development of sustainable treatment technologies, and utilization of the thermochemical platform for lignocellulosic biomass-based biofuel production.

Mika Sillanpää received his M.Sc. (Eng.) in Chemical Engineering and D.Sc. (Eng.) degrees from the Helsinki University of Technology (presently known as Aalto University) where he also completed an MBA degree in 2013. His research work is closely related to chemical treatment in environmental engineering and environmental monitoring and analysis with extensive focus on adsorption, photocatalysis, electrochemical treatment, membrane biological processes and advanced oxidation processes as well as ion mobility spectrometry, chromatographic methods, electrochemical sensor development and real-time monitoring.

© 2021 Wiley-VCH GmbH